Parameterization method for unstable manifolds of standing waves on the line

Blake Barker * [1], J.D. Mireles James † [2], and Jalen Morgan ‡ [3]

[1,3]Brigham Young University, Mathematics Department
[2]Florida Atlantic University, Department of Mathematical Sciences

August 19, 2019

Abstract

We consider a linearly unstable standing wave solution of a parabolic partial differential equation (PDE) on the real line and develop a high order method for polynomial approximation of the local unstable manifold. The unstable manifold describes the breakdown of the nonlinear wave after the loss of stability. Our method is based on the parameterization method for invariant manifolds and studies an invariance equation describing a local chart map. This invariance equation is a PDE posed on the product of a disk and the line. The dimension of the disk is equal to the Morse index of the wave. We develop a formal series solution for the invariance equation, and show that the coefficients of the series solve certain boundary value problems (BVPs) on the line. We solve these BVPs numerically to any desired order. The result is a polynomial describing the dynamics of the PDE in a macroscopic neighborhood of the unstable standing wave. The method is implemented for a number of example problems. Truncation/numerical errors are quantified via a-posteriori indicators.

1 Introduction

Understanding the emergence and evolution of coherent structures is a fundamental challenge in applied mathematics, and a rich class of examples come from partial differential equations (PDEs) posed on the entire real line. Traveling waves are an important special class of solutions where one looks for a fixed wave profile propagating with fixed wave speed. Waves with zero speed are known as standing waves. Questions about the existence and

*Email: blake@mathematics.byu.edu
†J.D.M.J partially supported by NSF grant DMS 1813501 Email: jmirelesjames@fau.edu
‡Email: jalen.morgan@byu.edu

shape of one-dimensional traveling waves are equivalent to questions about the existence and shape of certain homoclinic/heteroclinic connecting orbits for finite dimensional vector fields. This observation leads to a dramatic reduction in the dimension of the problem and forges deep connections between the theory of nonlinear waves and the qualitative theory of dynamical systems.

After a nonlinear wave is located a natural next step is to consider its stability. That is, what happens to patterns starting near but not on the traveling wave? While stable waves are observed in a wide variety of natural systems and mathematical models, unstable waves are not attracting hence are difficult to observe directly. Nevertheless, insights from the qualitative theory of dynamical systems suggest that unstable waves play an important role in the organization of global dynamics. For example changes in stability are important for understanding spontaneous emergence and bifurcation of patterns. Moreover, unstable orbits are dense in chaotic attractors and understanding them is important for understanding spatiotemporal complexity.

Numerical analysis of traveling waves is a growing area, and within the last decade several tools for locating and modeling unstable waves have been developed. Software packages such as STABLAB [1] facilitate stability calculations by means of the Evans function, the zeros of which are the eigenvalues of the linearized wave. More recently, additional functionality which assists in the automatic derivation of finite difference methods has been added to STABLAB. The tools in STABLAB are used in the present work to compute traveling wave profiles, to analyze spectral stability, and to simulate the flow generated by the PDE.

A next natural step in this program is to study nonlinear instabilities, and the organizing concept is that of the unstable manifold. The unstable manifold describes how nearby solutions move away from the traveling wave in the fully nonlinear problem. This description is critical for understanding the emergence and break up of patterns in the full nonlinear problem.

We develop a new approach for computing high order Taylor approximations of the unstable manifold attached to a traveling wave. Our approach is based on the parameterization method of Cabré, Fontich, and de la Llave [2, 3, 4]. The parameterization method provides a general functional analytic framework for studying invariant manifolds in a number of different contexts and applications. The method is constructive and leads to efficient and accurate numerics. The parameterization is not required to be the graph of a function over an eigenspace, hence the method can follow folds in the embedding. In addition to providing the embedding, the parameterization method also recovers explicitly the dynamics on the manifold.

Following the works just cited – which focus on manifolds attached to fixed points of infinite dimensional maps – the parameterization method has been extended by a number of authors to more general situations such as whiskered tori [5, 6, 7, 8, 9, 10, 11], quasi-periodic invariant manifolds in infinite dimensional problems [12, 13, 14], and to stable/unstable manifolds attached to periodic orbits of ordinary differential equations [15, 11, 16, 17, 18, 19] to cite only a few developments. We refer to the book of [20] for a much more complete

overview of the literature. We only mention that several recent papers develop numerical approximation schemes for unstable manifolds in infinite dimensional dynamical systems. See for example the work of [21] on unstable manifolds attached to equilibrium and periodic orbits of delay differential equations, the work of [22] on unstable manifolds attached to equilibrium solutions of one dimensional scalar parabolic PDE posed on compact intervals, and the extension to planar polygonal domains using finite element methods [23].

The present work generalizes the parameterization method to the setting of unstable manifolds attached to standing waves for parabolic PDEs on the line. The main idea is to look for a parameterization of a local unstable manifold satisfying a certain invariance equation. We derive a formal series solution for this invariance equation and show that the coefficients are given by a recursive scheme. The main observation is that recursive system of equations describing the Taylor coefficients are themselves linear boundary value problems (BVPs) - the so called *homological equations* – with each BVP formulated on the line. Recursive numerical solution of these linear BVPs up to some finite order N provides a polynomial approximation of the parameterization. The parameterization conjugates the dynamics on the manifold to the linear dynamics given by the unstable eigenvalues. Checking the conjugacy provides an a-posteriori measure of the truncation/numerical error.

We implement the scheme for three systems with well known unstable standing waves: the Nagumo equation, the Gray Scott system, and a nonlinear Shrödinger's equation. We compute the manifold to high order and verify its accuracy using automatic finite difference code courtesy of Todd and Morgan [24]. In addition, we perform an a-posteriori error analysis of each calculation. The MATLAB code is freely available at

`Github.com/finitediff/Unstable-Manifold`

Before concluding this introduction we remark that numerical methods for computing invariant manifolds for PDEs and other infinite dimensional systems have a long history and rich literature. While a thorough review of the literature is far beyond the scope of the present work, we would like to mention – in addition to the references cited above – a few papers which could serve as an entry point to this vast literature. We refer for example to the works of [25, 26, 27, 28] on heteroclinic and homoclinic phenomena, the works of [29, 30, 31, 32, 33] for a description of the organizing role of unstable periodic orbits and their invariant manifolds in the study of turbulence, to the works of [34, 35, 36, 37, 38] on numerical methods for inertial manifold reduciton, the works of [39, 40, 41, 42] on numerical methods for center manifold reduciton, the woks of [43, 44, 45, 46, 47] on efficient numerical calculation of spectral submanifolds, and the work of [48, 49, 50, 51, 52, 53] on the role of invariant manifolds in delay differential equations. Again, we stress that this list barely scratches the surface of the literature, and that the interested reader will find much of interest by consulting the references of the papers just mentioned.

The remainder of the paper is organized as follows. After reviewing some requisite background material and presenting the main example problems in Section 2, we describe in Section 3 the parameterization method for standing waves of PDEs on the line. We place

a heavy emphasis on formal series solutions of the invariance equation for the main example applications – that is, we emphisize the derivation of the homological equations in concrete problems. In Section 4 we describe and implement numerical procedures for solving the homological equations and profiling the results. Some conclusions and suggestions for future work are discussed in 5.

2 Background

We begin by reviewing some now standard results about the parameterization method. In particular the invariance equation is given and its basic implications discussed. This material comprises only a few pages and is included so that the present work may serve as a stand alone introduction to the reader unfamiliar with these developments.

Similarly we describe some classical material about computation and stability analysis of traveling wave solutions for PDEs on the line. This material underpins our entire approach. We conclude the section by presenting the three main example applications studied in this present work: Nagumo's Equation, the Gray-Scott system, and a nonlinear Schrödinger equation. For each system we provide a non-trivial unstable standing wave solution for further analysis later in the paper.

The reader familiar with the topics reviewed in this Section is encouraged to skip ahead to Section 3. Indeed, many readers will want to skim the present section and refer back to it only as needed.

2.1 Overview of the parameterization method for unstable manifolds of vector fields

Let $\mathcal{H}$ be a Hilbert space, $\mathcal{D} \subset \mathcal{H}$ be a dense subset. For a smooth mapping $F \colon \mathcal{D} \to \mathcal{H}$ we are interested in the differential equation

$$\frac{\partial}{\partial t} u(t) = F(u(t)).$$

We are interested in the dynamics near an equilibrium solution $u_* \in \mathcal{D}$. Observe that u_* is an equilibrium solution if

$$F(u_*) = 0.$$

Assume that $A = DF(u_*)$ has finite Morse index. More precisely, we require that A has at most finitely many unstable eigenvalues each with only finite multiplicity. We write $\lambda_1, \ldots, \lambda_M$ to denote the unstable eigenvalues and order them so that

$$0 < \operatorname{real}(\lambda_1) \leq \ldots \leq \operatorname{real}(\lambda_M).$$

In the present work we assume for the sake of simplicity that each unstable eigenvalue has multiplicity one. This assumption can be removed – for example see [2, 54] – however in the

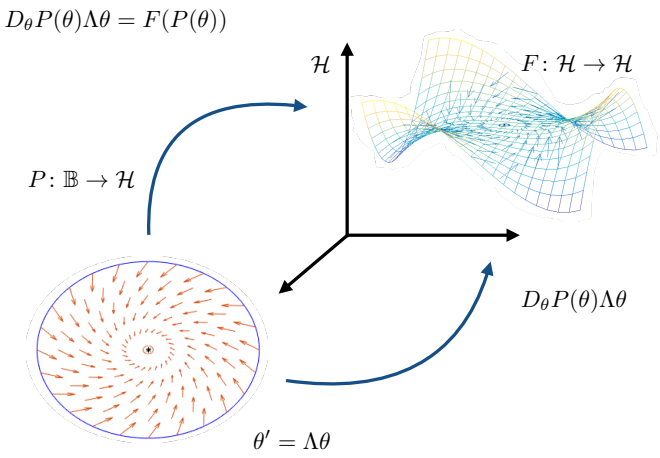

Figure 1: Geometric interpretation of the invariance equation. $D_\theta P$ maps the vector field $\Lambda\theta$ in $\mathbb{B}$ onto the image of P. This push forward should match that given vector field F in the image of P. If the two vector fields match then they generate the same dynamics (orbits).

present work we avoid these technicalities. Choose $\xi_1, \ldots, \xi_M \in \mathcal{D}$ associated eigenvectors. More precisely we require that

$$DF(u_*)\xi_j = \lambda_j \xi_j, \qquad 1 \leq j \leq M.$$

If $M \geq 0$ the equilibrium u_* is said to be spectrally unstable, and we are interested in parameterization of the M dimensional unstable manifold attached to u_*. To be more precise, let $r_1, \ldots, r_M > 0$ and define $\mathbb{B} = [-r_1, r_1] \times \ldots \times [-r_M, r_M]$. Consider a smooth function $P\colon \mathbb{B} \to \mathcal{H}$ having that

$$P(0) = u_*, \tag{1}$$

$$\partial_j P(0) = \xi_j, \qquad 1 \leq j \leq M. \tag{2}$$

Such a P is tangent to the unstable manifold, and we would like to impose additional constraints so that

$$P(\mathbb{B}) \subset W^u(u_*).$$

Write

$$\Lambda = \begin{pmatrix} \lambda_1 & \ldots & 0 \\ \vdots & \ddots & \vdots \\ 0 & \ldots & \lambda_M \end{pmatrix}.$$

The parameterization method looks for a P which, in addition to satisfying the constraint Equations (1) and (2), is also a solution of the *invariance equation*

$$F(P(\theta)) = DP(\theta)\Lambda\theta, \qquad \text{for all } \theta \in \text{interior}\,(\mathbb{B})\,. \tag{3}$$

Figure 1 illuminates the meaning of Equation (3), which is asking that the push forward of the linear vector field Λ by DP matches the vector field F restricted to the image of P. Loosely speaking, since the two vector fields match on the image of P they must generate the same dynamics – with the dynamics generated by Λ well understood. Then P maps orbits of Λ in $\mathbb{B}$ to orbits of F on the image of P, as we will show below. Since P maps orbits to orbits, Equation (3) is also called an infinitesimal conjugacy equation. The orbit correspondence is illustrated in Figure 2, and the observations of the preceding paragraph are made precise by the following lemma. For the sake of simplicity we suppose that the unstable eigenvalues are real. This restriction can be lifted and complex conjugate eigenvalues handled as described in [55], and we actually consider this case in Section 2.3 The elementary proof of the lemma is found in [23].

Lemma 2.1 (Orbit correspondence)**.** *Assume that the unstable eigenvalues $\lambda_1, \ldots, \lambda_M$ are real and distinct. Suppose that $P\colon \mathbb{B} \to \mathcal{H}$ satisfies the first order constraints of Equations* (1) *and* (2)*, and that P is a smooth solution of Equation* (3) *on interior*$(\mathbb{B}) = (-r_1, r_1) \times \ldots \times (-r_M, r_M)$*. Then P parameterizes a local unstable manifold for u_*.*

Suppose that F generates a flow Φ near u_*. In this case Lemma 2.1 the result of the Lemma can be restated by saying that P satisfies the flow conjugacy

$$P(e^{\Lambda t}\theta) = \Phi(P(\theta), t),$$

for all t such that $e^{\Lambda t}\theta \in \mathbb{B}$. So, P conjugates the flow generated by Λ to the flow generated by F. In this sense, P recovers the dynamics on the parameterized manifold in addition to the embedding.

Lemma 2.1 explains our interest in the invariance Equation (3). Sections 2.1 and 4 respectively develop formal series methods for solving (3) as well as numerical implementation of the soluitons.

2.2 Computing profiles, eigenvalues, and eigenfunctions

Let us fix for a moment a specific class of examples. With $f\colon \mathbb{R} \to \mathbb{R}$ a smooth function consider the parabolic scalar reaction diffusion equations in one spatial dimension given by

$$\frac{\partial}{\partial t}u(x,t) = \frac{\partial^2}{\partial x^2}u(x,t) + f(u(x,t)), \qquad x \in \mathbb{R}, t \geq 0. \tag{4}$$

A standing wave solution is a smooth function $u_*\colon \mathbb{R} \to \mathbb{R}$ satisfying

$$u_*''(x) + f(u_*(x)) = 0, \tag{5}$$

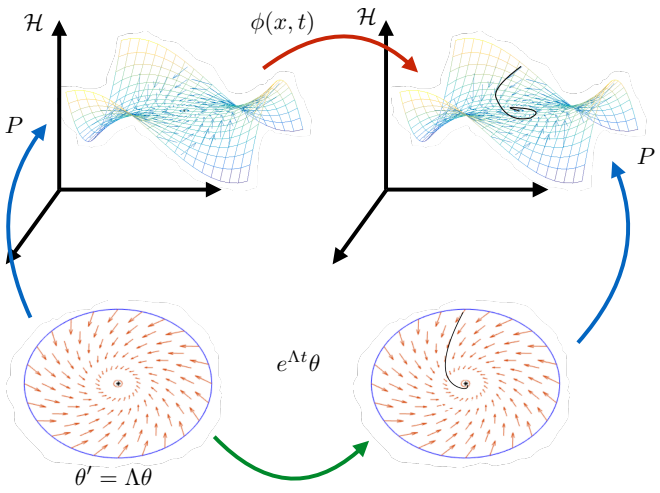

Figure 2: Flow conjugacy induced by the invariance Equation. The orbits of $e^{\Lambda t}$ accumulate in backwards time to the origin in $\mathbb{B}$. The parameterization P lifts these orbits to curves which are themselves orbits in $\mathcal{H}$. The orbits in $\mathcal{H}$ accumulate at the equilibrium u_*, so that the image of P is a local unstable manifold for u_*. (3)

where $' := d/dx$ denotes differentiation with respect to the spatial variable. We refer to Equation (5) as the (standing wave) profile equation. In the present work we are interested in standing waves which are asymptotically constant and require

$$\lim_{x\to-\infty} u_*(x) = C_- \qquad \text{and} \qquad \lim_{x\to\infty} u_*(x) = C_+,$$

for some constants $C_\pm \in \mathbb{R}$.

By a standard change of variables $u_1 = u, u_2 = u'$ we rewrite the profile equation as a nonlinear system of first order ODEs

$$\begin{aligned} u_1' &= u_2 \\ u_2' &= -f(u_2). \end{aligned}$$

Observe an equilibrium solution of this system has $u_2 = 0$ and

$$f(u_1) = 0.$$

Suppose now that a_0 and a_1 are (not necessarily distinct) zeros of f, so that $(a_0, 0)$ and $(a_1, 0)$ are equilibrium solutions of the ODE system. If $u_1(t), u_2(t)$ is a non-constant solution of the profile system with

$$\lim_{t\to-\infty} u_1(t) = a_0, \qquad \lim_{t\to-\infty} u_2(t) = 0, \qquad \lim_{t\to\infty} u_1(t) = a_1, \qquad \text{and} \qquad \lim_{t\to\infty} u_2(t) = 0,$$

then $u_*(x) = u_1(x)$ is the profile of a standing wave solution of Equation (4) with $C_- = a_0$ and $C_+ = a_1$. The discussion extends naturally to systems of reaction diffusion PDEs with one spatial dimension, and to parabolic PDEs with more general diffusion operators. For just a few examples, see [56, 57, 58, 59, 60]

Looking for a standing wave reduces the problem of finding solutions of the PDE to the problem of finding heteroclinic/homoclinic connecting orbits for an ODE: the profile equations. The desired connecting orbits are computed numerically by projecting the boundary conditions onto the stable/unstable eigenspace at the equilibrium solution and solving the resulting two point boundary value problem. This numerical procedure is discussed in detail in [61, 62].

Stability of the standing wave is reduced to the study of certain ODEs as follows. Consideration of the eigenvalue problem for the PDE linearized about the traveling wave solution leads to

$$w''(x) + f'(u_*(x))w(x) = \lambda w(x), \qquad x \in \mathbb{R}.$$

Define the λ dependent matrices

$$A_-(\lambda) = \begin{pmatrix} 0 & 1 \\ \lambda - f'(a_0) & 0 \end{pmatrix}$$

$$A_+(\lambda) = \begin{pmatrix} 0 & 1 \\ \lambda - f'(a_1) & 0 \end{pmatrix}$$

and the non-constant matrix

$$A(x, \lambda) = \begin{pmatrix} 0 & 1 \\ \lambda - f'(u_*(x)) & 0 \end{pmatrix}.$$

Letting $W = (w, w')$ we look for $\lambda \in \mathbb{C}$ so that the non-autonomous linear equation

$$W(x)' = A(\lambda, x)W(x),$$

has solutions asymptotic to the stable eigenspace of A_+ and the unstable eigenspace of A_- as $t \to \pm\infty$ respectively. So, linear stability of the standing wave is reduced to solution of a certain two point boundary value problem on the line.

In the present work the eigenvalues λ are found as zeros of the Evans function, an infinite dimensional generalization of the determinant of a finite dimensional square matrix. The Evans function is discussed from a numerical point of view in [63, 64]. We employ the numerical package STABLAB [1] for the Evans function calculations in the present work.

To numerically approximate the associated eigenfunction, we double the size of the Evans ODE system by making a linear change of coordinates to express the solution that corresponds to the interval $[0, L]$ on the interval $[-L, 0]$, where $L \gg 1$. This allows us to give a norm condition on the eigenfunction at $x = 0$ while still using MatLab's two-point

boundary value solver bvp5c, which uses the four-stage Lobatto IIIa formula. The boundary value problem is thus,

$$\begin{aligned} \begin{pmatrix} W'(x) \\ Z'(x) \end{pmatrix} &= \begin{pmatrix} A(x;\lambda)W(x) \\ A(x+L;\lambda)Z(x) \end{pmatrix}, \\ P_s\ W(-L) = 0, \quad P_u\ Z(0) = 0, \quad ||W(0)||^2 = 1, \quad x &\in [-L, 0], \end{aligned} \tag{6}$$

where P_s is the projection onto the stable subspace of $A_-(\lambda)$, and P_u is the projection onto the unstable subspace of $A_+(\lambda)$, where $A_\pm(\lambda) := \lim_{x\to\pm\infty} A(x;\lambda)$. The spectral parameter λ is treated as a free variable, which allows us to provide the norm condition on the eigenfunction. To provide an initial guess for the eigenvalue, we solve for the eigenvalue using Evans function root solving routines built into STABLAB; see [1]. We use $\mathrm{sech}(x)$ and its derivatives as the initial guess for W and Z. See [65] for more details about how one can solve for an eigenfunction in this setting.

Remark 2.2 (Non-zero wave speed)**.** The discussion above generalizes substantially by considering traveling waves. To be more precise, suppose that we look for solutions of Equation (4) having the form $u(x,t) = u_*(x-ct)$. That is, we seek out waves with a fixed shape u_* moving at a constant speed $c \neq 0$. This is referred to as *the traveling wave ansatz*, and upon substituting it into Equation (4) we arrive at the system

$$u_*'' - cu_*' + f(u_*) = 0,$$

where $'$ denotes differentiation with respect to the variable $\tau = x - ct$. Imposing the same boundary conditions as before we are once again led to a system of ODEs whose heteroclinic and homoclinic solutions must be analyzed. We remark that the parameterization method for standing waves developed in Section 3 extends in a natural way to unstable manifolds for more general traveling waves simply by studying the standing waves of the transformed system.

2.3 Example systems: profiles and eigendata

In this section we describe the three models used in the present work. For each system we consider a standing wave profile and examine the stability via the Evans Function. The first model is Nagumo's equation, for which an explicit pulse solution, explicit eigenvalue, and explicit eigenfunction are known. The second model, the Gray-Scott system, also has explicit solutions for unstable standing waves, but explicit solutions for its eigenfunctions are not known. The third system, Shrödinger's equation, is known to exhibit a Hopf bifurcation resulting in oscillating eigenfunctions associated with complex conjugate eigenvalues. The Gray-Scott and Schrödinger models illustrate that our method applies to systems as well as scalar equations. The Schrödinger model further illustrates the computation of a two dimensional unstable manifold.

2.3.1 Nagumo Equation

The Nagumo equation in one spatial dimension is given by,

$$u_t = u_{xx} - u + u^3, \tag{7}$$

where $u(x,t) : \mathbb{R} \times (0,\infty) \to \mathbb{R}$. The profile equation for a standing wave is

$$u'' - u + u^3 = 0,$$

which leads to the first order system

$$\begin{aligned} u_1' &= u_2 \\ u_2' &= u_1 - u_1^3. \end{aligned}$$

The Nagumo equation has an unstable standing wave solution given by

$$u_*(x) = u_1(x) = \sqrt{2}\,\operatorname{sech}(x).$$

Linearizing (7) about the wave u_* and looking for separated solutions (that is, ignoring the continuous spectrum) yields the eigenvalue problem

$$\xi''(x) - \xi(x) + 3u_*(x)^2\xi(x) = \lambda\xi(x), \quad \lim_{x\to\pm\infty} \xi(x) = 0, \quad ||\xi|| \neq 0. \tag{8}$$

A solution to (8) for the unique unstable eigenvalue $\lambda = 3$ is given by the eigenfunction,

$$\xi(x) = \begin{cases} e^{2x}(2 - 2\tanh(x) - \operatorname{sech}^2(x)) & \text{if } x \geq 0 \\ e^{-2x}(2 + 2\tanh(x) - \operatorname{sech}^2(x)) & \text{if } x < 0. \end{cases}$$

, can be seen in Figure 3. The profile and eigenfunction for Nagumo's equation are plotted in Figure 3.

2.3.2 Gray-Scott

The Gray Scott equations in one spatial dimension are given by

$$\begin{aligned} u_t &= u_{xx} - uv^2 + \alpha(1-u), \\ v_t &= v_{xx} + uv^2/\gamma - v/\gamma, \end{aligned} \tag{9}$$

where $u, v : \mathbb{R} \times (0,\infty) \to \mathbb{R}$, and $\alpha, \gamma > 0$ are parameters. The equations model a cubic autocatalytic reaction without stirring [66, 67, 68]. The profile equations for a standing wave solution are

$$u'' = uv^2 - \alpha(1-u), \quad v'' = \frac{1}{\gamma}(v - uv^2). \tag{10}$$

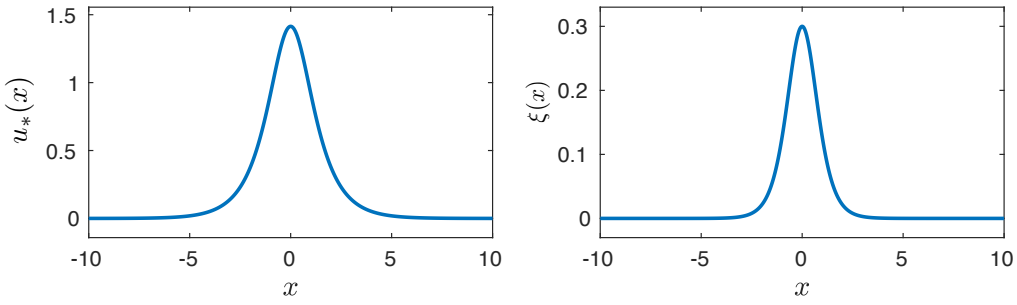

Figure 3: The Nagumo equation profile, $u_*(x)$, and eigenfunction, $\xi(x)$ associated with the unstable eigenvalue $\lambda = 3$.

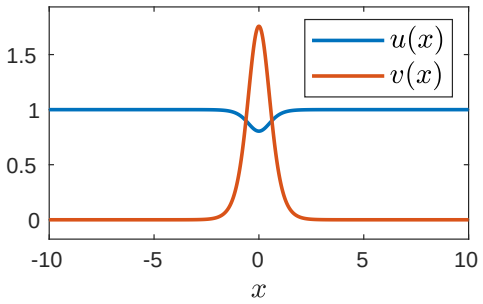

Figure 4: Standing wave solution for the Gray-Scott equations.

We take $\alpha\gamma = 1$ and $0 < \gamma < \frac{2}{9}$, as for these parameters there is a known explicit solution (see [67]) for the profile equations given by

$$\begin{aligned} u_*(x) &= 1 - \frac{3\gamma}{1 + Q\cosh(x/\sqrt{\gamma})}, \\ v_*(x) &= \frac{3}{1 + Q\cosh(x/\sqrt{\gamma})}, \end{aligned} \tag{11}$$

where $Q := \sqrt{1 - 9\gamma/2}$. These solutions were shown to be unstable in [69]. We select values of $\alpha = 9$ and $\gamma = \frac{1}{9}$. The corresponding profile is shown in Figure 4.

Linearizing equations (9) about the profile (u_*, v_*), and looking for separated solutions, we arrive at the eigenvalue problem

$$\begin{aligned} \xi'' - v_*^2\xi - 2u_*v_*\eta - \alpha\xi &= \lambda\xi, \\ \eta'' + \frac{v_*^2}{\gamma}\xi + \frac{2}{\gamma}u_*v_*\eta - \frac{1}{\gamma}\eta &= \lambda\eta, \end{aligned}$$

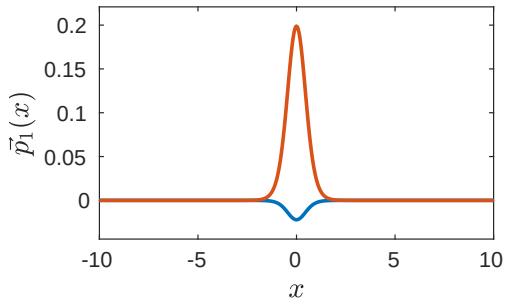

Figure 5: The Gray-Scott eigenfunctions, $\xi(x)$ and $\eta(x)$ – red (top) and blue (bottom) respectively.

which upon rearranging terms becomes the second order system,

$$\xi'' = v_*^2\xi + 2u_*v_*\eta + \alpha\xi + \lambda\xi, \tag{12}$$

$$\eta'' = -\frac{v_*^2}{\gamma}\xi - \frac{2}{\gamma}u_*v_*\eta + \frac{1}{\gamma}\eta + \lambda\eta. \tag{13}$$

We note that, due to the symmetry of u_* and v_*, eigenfunctions may be even or odd functions of $x \in \mathbb{R}$. We introduce the variables $\xi_1 = \xi, \xi_2 = \xi', \eta_1 = \eta, \eta_2 = \eta'$ and write (12) as a first order system $W'(x;\lambda) = A(x;\lambda)W(x;\lambda)$ as follows,

$$\begin{pmatrix} \xi_1' \\ \xi_2' \\ \eta_1' \\ \eta_2' \end{pmatrix} = \begin{pmatrix} 0 & 1 & 0 & 0 \\ \lambda + v_*^2 + \alpha & 0 & 2u_*v_* & 0 \\ 0 & 0 & 0 & 1 \\ -v_*^2/\gamma & 0 & \lambda + (1 - 2u_*v_*)/\gamma & 0 \end{pmatrix} \begin{pmatrix} \xi_1 \\ \xi_2 \\ \eta_1 \\ \eta_2 \end{pmatrix}. \tag{14}$$

The asymptotic matrices $A_\pm := \lim_{x\to\pm\infty} A(x;\lambda)$ are given by

$$A_\pm(\lambda) = \begin{pmatrix} 0 & 1 & 0 & 0 \\ \lambda + \alpha & 0 & 0 & 0 \\ 0 & 0 & 0 & 1 \\ 0 & 0 & \lambda + 1/\gamma & 0 \end{pmatrix}. \tag{15}$$

The eigenvalues of $A_\pm$ are given by $\mu_1^\pm = \pm\sqrt{\lambda + \alpha}$ and $\mu_2^\pm = \pm\sqrt{\lambda + 1/\gamma}$. The associated eigenvectors are given by $v_1^\pm = (1, \mu_1^\pm, 0, 0)^T$ and $v_2^\pm = (0, 0, 1, \mu_2^\pm)^T$. Using these eigenvectors to create projective boundary conditions, we solve for the eigenfunction as described in Section 2.2.

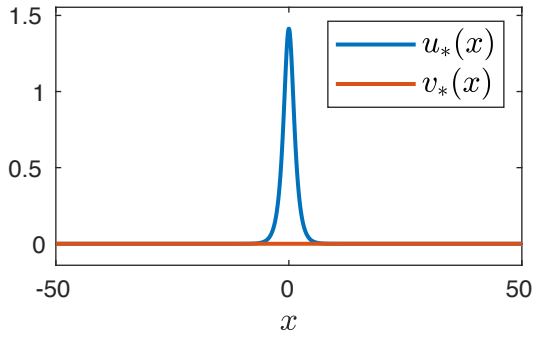

Figure 6: Profile for PNLS. The blue (top) line corresponds to the component u_*, and the orange (bottom) line to the component v_*.

2.3.3 Nonlinear Shrödinger Equations

The rescaled, parametrically-forced nonlinear Shrödinger equation (PNLS) in one spatial dimension is given by,

$$\begin{aligned} u_t &= -v_{xx} + \mu v - v(v^2 + u^2), \\ v_t &= u_{xx} - u + u(v^2 + u^2) - 2\nu v, \end{aligned} \tag{16}$$

where u and v represent respectively the real and imaginary part of the dependent variable of the rescaled PNLS, and μ and ν are rescaled coefficients; see [70] for details. It was shown in [70] that Hopf bifurcations of a pulse solution exist in PNLS.

The system has a stationary pulse equilibrium given by $(u_*, v_*) = (\mathrm{sech}(x), 0)$ solving the profile equation

$$\begin{aligned} -v'' + \mu v - v^3 - vu^2 &= 0, \\ u'' - u - 2\nu v + uv^2 + u^3 &= 0; \end{aligned} \tag{17}$$

see Figure 6.

Linearizing about the profile leads to the eigenvalue problem

$$\begin{aligned} -\eta'' + \mu\eta - 3v_*^2\eta - u_*^2\eta - 2u_*v_*\xi &= \lambda\xi \\ \xi'' - \xi - 2\nu\eta + v_*^2\xi + 2u_*v_*\eta + 3u_*^2\xi &= \lambda\eta. \end{aligned} \tag{18}$$

We fix parameters $\mu = 0.3957$ and $\nu = 0.1745$, which correspond to $a = 4$ and $\gamma = 2$ in [70]. We solve for one of the eigenvalue-eigenfunction pairs of PNLS using the method described in Section 2.2, and then we obtain the other eigen pair by taking the complex conjugate of the first. There are a pair of complex conjugate unstable eigenvalues $\lambda_{1,2} \approx 0.0557 \pm 1.3053i$. We plot the real and imaginary parts of the associated eigenfunctions in Figure 7.

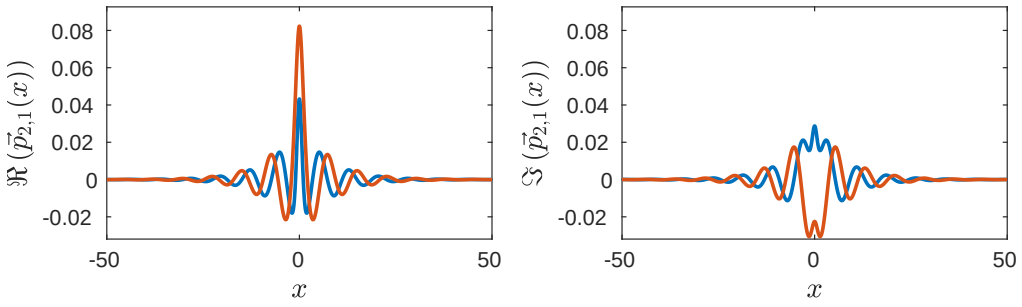

Figure 7: The real and imaginary part of the eigenfunctions corresponding to the complex conjugate pair of eigenvalues $\lambda_{1,2} = 0.0557 \pm 1.3053i$. Red corresponds to $\xi(x)$, and blue to $\eta(x)$.

3 Unstable manifolds for standing waves: formal series calculations

In this section, we derive the formal derivation of the homological equations.

3.1 Cauchy products of power series

Derivation of homological equations in the applications below relies on some formal power series manipulations. These calculations are much cleaner if we introduce a little notation. In particular, since our example systems are nonlinear, products of power series are a critical operation. In the present work we consider polynomial systems with only quadratic and cubic nonlinearities. We remark that higher degree polynomials are treated similarly. Moreover, using techniques from automatic differentiation for power series it is possible to transform non-polynomial systems into polynomial systems of a larger number of variables. For explicit examples of this procedure for parabolic PDEs see [23]. A more abstract discussion is found in Chapter 2 of [20].

For the present work it is enough to consider the Cauchy product of two or three power series in one or two variables. Consider then the three power series of a single variable given by

$$P(\theta) = \sum_{n=0}^{\infty} p_n \theta^n,$$

$$Q(\theta) = \sum_{n=0}^{\infty} q_n \theta^n,$$

and

$$R(\theta) = \sum_{n=0}^{\infty} r_n \theta^n.$$

The point wise products of $P \cdot Q$ and $P \cdot Q \cdot R$ are expressed as power series via the Cauchy product formulas

$$(P \cdot Q)(\theta) = \sum_{n=0}^{\infty} (p * q)_n \theta^n,$$

and

$$(P \cdot Q \cdot R)(\theta) = \sum_{n=0}^{\infty} (p * q * r)_n \theta^n,$$

where

$$(p * q)_n = \sum_{j=0}^{n} p_{n-j} q_j,$$

and

$$(p * q * r)_n = \sum_{j=0}^{n} \sum_{k=0}^{j} p_{n-j} q_{j-k} r_k.$$

Suppose we want to isolate the highest order terms from the Cauchy products. We have that

$$\begin{aligned}
(p * q)_n &= \sum_{j=0}^{n} p_{n-j} q_j \\
&= p_0 q_n + q_0 p_n + \sum_{j=1}^{n-1} p_{n-j} q_j \\
&= p_0 q_n + q_0 p_n + (p \hat{*} q)_n,
\end{aligned}$$

where we define

$$(p \hat{*} q)_n = \sum_{j=1}^{n-1} p_{n-j} q_j.$$

For the cubic term we have that

$$(p * q * r)_n = p_0 q_0 r_n + q_0 r_0 p_n + p_0 r_0 q_n + (p \hat{*} q \hat{*} r)_n,$$

where

$$(p \hat{*} q \hat{*} r)_n = \sum_{j=0}^{n} \sum_{k=0}^{j} \hat{\delta}_{njk} p_{n-j} q_{j-k} r_k$$

where the term $\hat{\delta}_{njk}$ is defined by

$$\hat{\delta}_{jk}^{nj} = \begin{cases} 0 & \text{if } j = k = 0 \\ 0 & \text{if } j = k = n \\ 0 & \text{if } k = 0 \text{ and } j = n \\ 1 & \text{otherwise} \end{cases},$$

and appears so that terms of order n are removed from the Cauchy product. The point is that the so called "hat products" do not depend on terms of order n.

Similarly, consider three power series of two variables

$$P(\theta_1, \theta_2) = \sum_{n=0}^{\infty} \sum_{m=0}^{\infty} p_{mn} \theta_1^m \theta_2^n,$$

$$Q(\theta_1, \theta_2) = \sum_{n=0}^{\infty} \sum_{m=0}^{\infty} q_{mn} \theta_1^m \theta_2^n,$$

and

$$R(\theta_1, \theta_2) = \sum_{n=0}^{\infty} \sum_{m=0}^{\infty} r_{mn} \theta_1^m \theta_2^n.$$

Define the Cauchy products

$$(P \cdot Q)(\theta_1, \theta_2) = \sum_{n=0}^{\infty} \sum_{m=0}^{\infty} (p * q)_{mn} \theta_1^m \theta_2^n$$

and

$$(P \cdot Q \cdot R)(\theta_1, \theta_2) = \sum_{n=0}^{\infty} \sum_{m=0}^{\infty} (p * q * r)_{mn} \theta_1^m \theta_2^n$$

where

$$(p * q)_{mn} = \sum_{i=0}^{m} \sum_{j=0}^{m} p_{m-i,n-j} q_{ij},$$

and

$$(p * q * r)_{mn} = \sum_{i=0}^{m} \sum_{j=0}^{i} \sum_{k=0}^{n} \sum_{l=0}^{k} p_{m-i,n-k} q_{i-j,k-l} r_{jl}.$$

In this case we have that

$$(p * q)_{mn} = p_{00} q_{mn} + q_{00} p_{mn} + (p \hat{*} q)_{mn},$$

and

$$(p * q * r)_{mn} = p_{00} q_{00} r_{mn} + p_{00} r_{00} q_{mn} + q_{00} r_{00} p_{mn} + (p \hat{*} q \hat{*} r)_{mn}$$

where

$$(p\hat{*}q)_{mn} = \sum_{i=0}^{m}\sum_{j=0}^{n} \hat{\delta}^{nj}_{mi} p_{m-i,n-j} q_{ij},$$

and

$$(p\hat{*}q\hat{*}r)_{mn} = \sum_{i=0}^{m}\sum_{j=0}^{i}\sum_{k=0}^{n}\sum_{l=0}^{k} \hat{\delta}^{nkl}_{mij} p_{m-i,n-k} q_{i-j,k-l} r_{jl},$$

with

$$\hat{\delta}^{nj}_{mi} = \begin{cases} 0 & \text{if } i = j = 0 \\ 0 & \text{if } i = m \text{ and } j = n \\ 1 & \text{otherwise} \end{cases}$$

and

$$\hat{\delta}^{nkl}_{mij} = \begin{cases} 0 & \text{if } i = k = 0 \\ 0 & \text{if } j = m \text{ and } l = n \\ 0 & \text{if } i = m, k = n, j = 0, \text{ and } l = 0 \\ 1 & \text{otherwise} \end{cases}.$$

3.2 Homological equations for standing waves

We now specialize the discussion of the parameterization method given in Section 2.1 to the case of the flow generated by a parabolic partial differential equation on the line. We think of Equation (4) as generating the Cauchy problem

$$u_t = F(u), \tag{19}$$

where for example the vector field F could be defined given by

$$F(u)(x) = \frac{\partial^2}{\partial x^2} u(x) + f(u(x)),$$

with u in an appropriate Hilbert space. (More general problems involving systems are considered in Section 4).

Suppose that $u_* \colon \mathbb{R} \to \mathbb{R}$ has

$$F(u_*) = \frac{\partial^2}{\partial x^2} u_*(x) + f(u_*(x)) = 0,$$

for all $x \in \mathbb{R}$. We say that u_* is an equilibrium solution of Equation (19), and note that an equilibrium solution u_* corresponds to a standing wave solution of Equation (4).

An eigenvalue eigenvector pair (ξ, λ) for the equilibrium u_*, is a solution of the eigenvalue problem

$$DF(u_*)\xi = \lambda\xi,$$

or more explicitly

$$\frac{\partial^2}{\partial x^2}\xi(x) + f'(u_*(x))\xi(x) = \lambda\xi(x), \tag{20}$$

for $x \in \mathbb{R}$. Following the discussion in Section 2.1, we assume that Equation 20 has exactly M solutions (ξ_j, λ_j) with real$(\lambda_j) > 0$ for $1 \leq j \leq M$ and $\xi_1, \ldots, \xi_M$ linearly independant. That is, assume that u_* has exactly M unstable eigenvalues each with multiplicity one.

Following the discussion of the parameterization method in Section 2.1 we make a power series ansatz

$$P(\theta_1, \ldots, \theta_M, x) = \sum_{m_1}^{\infty} \ldots \sum_{m_M=0}^{\infty} p_{m_1,\ldots,m_M}(x)\theta_1^{m_1} \ldots \theta_M^{m_M},$$

where each coefficient $p_{m_1,\ldots,m_M}(x)$ is in the same function space as u_*, and satisfies Dirchlet boundary conditions at infinity. Here we treat P as a formal series in θ and ignore the question of convergence.

Imposing the first order constraints of Equations (1) and (2) gives that

$$\begin{aligned} P(0, \ldots, 0, x) &= p_{0,\ldots,0} = u_*(x), \\ \frac{\partial}{\partial\theta_1}P(0, \ldots, 0, x) &= p_{1,0,\ldots,0} = \xi_1(x), \\ &\vdots \\ \frac{\partial}{\partial\theta_M}P(0, \ldots, 0, x) &= p_{0,0,\ldots,1} = \xi_M(x). \end{aligned}$$

To work out the form of the coefficients $p_{m_1,\ldots,m_M}$ of the formal series for $m_1 + \ldots + m_M \geq 2$ we insert power series ansatz into the Invariance Equation (3). Considering the two sides of the equation separately we have first that

$$\begin{aligned} D_\theta P(\theta, x)\Lambda\theta &= \lambda_1\theta_1\frac{\partial}{\partial\theta_1}P(\theta, x) + \ldots + \lambda_M\theta_M\frac{\partial}{\partial\theta_M}P(\theta, x) \\ &= \sum_{m_1=0}^{\infty} \ldots \sum_{m_M=0}^{\infty} (m_1\lambda_1 + \ldots + m_M\lambda_M)p_{m_1,\ldots,m_M}(x)\theta_1^{m_1} \ldots \theta_M^{m_M}, \end{aligned}$$

on the left and that

$$F(P(\theta, x)) = \frac{\partial^2}{\partial x^2}P(\theta, x) + f(P(\theta, x)),$$

on the right. Suppose that

$$f(P(\theta, x)) = \sum_{m_1}^{\infty} \ldots \sum_{m_M=0}^{\infty} q_{m_1,\ldots,m_M}(x)\theta_1^{m_1} \ldots \theta_M^{m_M},$$

where the coefficients $q_{m_1,\ldots,m_M}(x)$ depend on the coefficients $p_{m_1,\ldots,m_M}(x)$ in a problem dependent way. Then, (formally) we have that

$$F(P(\theta,x)) = \sum_{m_1=0}^{\infty} \ldots \sum_{m_M=0}^{\infty} \left(\frac{\partial^2}{\partial x^2} p_{m_1,\ldots,m_M}(x) + q_{m_1,\ldots,m_M}(x) \right) \theta_1^{m_1} \ldots \theta_M^{m_M}.$$

Matching like powers of θ leads to

$$\frac{\partial^2}{\partial x^2} p_{m_1,\ldots,m_M}(x) - (m_1\lambda_1 + \ldots + m_M\lambda_M) p_{m_1,\ldots,m_M}(x) = -q_{m_1,\ldots,m_M}(x),$$

for $m_1 + \ldots + m_M \geq 2$ (recall that the zero and first order coefficients are already known).

Now we want to isolate all the terms involving $p_{m_1,\ldots,m_M}(x)$ on one the left hand side of the equation, and obtain a BVP defining the $p_{m_1,\ldots,m_M}(x)$. The challenge is dealing with the fact that the right hand side of the equation depends in a complicated way on $p_{m_1,\ldots,m_M}(x)$.

Rather than continuing the discussion at this level of generality we we find it instructive to complete the remaining calculations in the context of specific application problems below. Before moving forward a remark about existence of solutions to the homological equations is in order. It can be shown that

$$q_{m_1,\ldots,m_M}(x) = f'(u_*(x)) p_{m_1,\ldots,m_M}(x) + R_{m_1,\ldots,m_M}(x),$$

where $R_{m_1,\ldots,m_M}(x)$ depends only on lower order terms. Then the *homological equation* defining $p_{m_1,\ldots,m_M}(x)$ has the form

$$\frac{\partial^2}{\partial x^2} p(x) + f'(u_*(x)) p(x) - (m_1\lambda_1 + \ldots + m_M\lambda_M) p(x) = -R_{m_1,\ldots,m_M}(x), \tag{21}$$

where $p(x) = p_{m_1,\ldots,m_M}(x)$. Equation (21) is a linear BVP for $p_{m_1,\ldots,m_M}(x)$, where we recall that $p_{m_1,\ldots,m_M}(x)$ should satisfy Dirchlet boundary conditions at infinity. Indeed this lets us rewrite the homological Equations (21) as

$$\left(DF(u_*) - (m_1\lambda_1 + \ldots + m_M\lambda_M)\mathrm{Id}\right) p(x) = -R_{m_1,\ldots,m_M}(x),$$

and we observe that the linear operator on the left hand side is boundedly invertible as long as $z = m_1\lambda_1 + \ldots + m_M\lambda_M$ is not an eigenvalue of $DF(u_*)$. Observing that $\mathrm{real}(z) > 0$ we see that this reduces to the scalar non-resonance condition

$$m_1\lambda_1 + \ldots + m_M\lambda_M \neq \lambda_j, \tag{22}$$

for $1 \leq j \leq M$. These are the finitely many non-resonance conditions which always one expects to appear in the parameterization method. They are the obstruction to the existence of a formal series conjugating the nonlinear dynamics to linear.

The non-resonance conditions of Equation (22) are valuable in practice as they are scalar conditions which warn us wether or not to proceed with the manifold calculation. Suppose for example that we have found the eigenvalues and are interested in computing the unstable manifold up to polynomial order N. Then we simply check the non-resonance for each multi-index $(m_1, \ldots, m_M) \in \mathbb{N}^N$ with $2 \leq m_1 + \ldots + m_M \leq N$. If there are no resonances to order N then we know in advance that we will be able to solve each of the homological equations defining the Taylor coefficients and we are confident with committing the computational resources.

Another observation is that if there are no resonances, then solutions of the homological equations are unique. Since the homological equations determine the coefficients for all orders greater than or equal to two, this says that once the first order data are chosen, the parameterization P solving Equation (3) is unique. But the only free choice in the first order data is the choice of the scalings of the eigenvectors. Put another way, the parameterization P is unique up to the choice of the eigenvector scaling. This non-uniqueness is exploited in numerical calculations where we use it to control the growth of the coefficients.

The remarks above are in direct analogy with the results obtained in [2] for fixed points of maps, and the formula in Equation (21) can be established by following the steps introduced there. More precisely, what one needs to do is find the explicit dependance of the $q_{m_1,\ldots,m_M}(x)$ on the $p_{m_1,\ldots,m_M}(x)$, but this can be worked out using the Taylor formula for the coefficients of the power series and the Faá di Bruno formula. The interested reader will find a similar argument carried out in detail in [21].

The general result given in Equation (21) is not needed for the present work, as in our experience it is much easier to derive the explicit form of the equation from scratch in a given application. In the next sections we discuss in more detail the methods used to obtain the equilibrium solution and to analyze its stability. Finally we remark that the entire discussion generalizes to systems of PDEs with only the obvious modifications, as illustrated in Section 4.

3.3 Homological equations for Nagumo's Equation

Since Nagumo's equation has one unstable eigenvalue λ, the unstable manifold is one dimensional and we look for $P(\theta, x)$ with $x \in \mathbb{R}$ and $\theta \in [-r, r]$ parameterizing the unstable manifold. (The value of r is a-priori unknown and is in fact set only after some numerical experimentation).

Assume that the parameterization has the power series expansion

$$P(\theta, x) = \sum_{n=0}^{\infty} p_n(x)\theta^n.$$

Imposing the first order conditions, $P(0, x) = p_0(x) = u_*(x)$ is the wave profile and $\frac{\partial}{\partial\theta}P(\theta, x)|_{\theta=0} = p_1(x) = \xi(x)$ is the eigenfunction.

The invariance equation for a one dimensional unstable manifold reduces to

$$\lambda\theta\frac{\partial}{\partial\theta}P(\theta,x)=F(P(\theta,x)),$$

where for the Nagumo equation

$$F(P(\theta,x))=\frac{\partial^2}{\partial x^2}P(\theta,x)-P(\theta,x)+P(\theta,x)^3.$$

We cary out the formal series calculation in some detail, for reasons which become clear by the end.

Substituting the power series ansatz into the invariance equation we have

$$\begin{aligned}\lambda\theta\frac{\partial}{\partial\theta}P(\theta,x)&=\lambda\theta\frac{\partial}{\partial\theta}\left(\sum_{n=0}^{\infty}p_n(x)\theta^n\right)\\&=\lambda\theta\sum_{n=0}^{\infty}np_n(x)\theta^{n-1}\\&=\sum_{n=0}^{\infty}\lambda np_n(x)\theta^n,\end{aligned}$$

on the left and

$$\begin{aligned}F(P(\theta,x))&=\frac{\partial^2}{\partial x^2}\left(\sum_{n=0}^{\infty}p_n(x)\theta^n\right)-\sum_{n=0}^{\infty}p_n(x)\theta^n+\left(\sum_{n=0}^{\infty}p_n(x)\theta^n\right)^3\\&=\sum_{n=0}^{\infty}p_n''(x)\theta^n-\sum_{n=0}^{\infty}p_n(x)\theta^n+\sum_{n=0}^{\infty}(p*p*p)_n(x)\theta^n\\&=\sum_{n=0}^{\infty}\left(p_n''(x)-p_n(x)+3p_0(x)^2p_n(x)+(p\hat{*}p\hat{*}p)_n(x)\right)\theta^n,\end{aligned}$$

on the right. By matching like powers we obtain that

$$\lambda np_n(x)=p_n''(x)-p_n(x)+3p_0(x)^2p_n(x)+(p\hat{*}p\hat{*}p)_n(x),$$

and isolating terms of order n on the left leads to the homological equation

$$p_n''(x)+\left(-1+3p_0(x)^2\right)p_n(x)-\lambda np_n(x)=-(p\hat{*}p\hat{*}p)_n(x). \tag{23}$$

We require that $p_n(x)\to 0$ as $x\to\pm\infty$.

Observe that Equation (23) does in fact have the form

$$\left[DF(p_0(x))-\lambda n\mathrm{Id}\right]p_n(x)=R_n(x),$$

with $R_n(x)$ is given explicitly by

$$R_n(x) = -(p\hat{*}p\hat{*}p)_n(x),$$

just as claimed in Section 3.2. The important point, in fact the entire reason for working through the formal calculation just given, is that we obtain explicitly the form of the right hand side $R_n(x)$.

Introducing the variable $q_n(x) = p_n'(x)$ we write (23) as a first order system, giving rise to the boundary value problem,

$$\begin{pmatrix} p_n' \\ q_n' \end{pmatrix} = \begin{pmatrix} 0 & 1 \\ 1+\lambda n - 3p_0^2 & 0 \end{pmatrix} \begin{pmatrix} p_n \\ q_n \end{pmatrix} - \begin{pmatrix} 0 \\ \sum_{k=0}^{n} \sum_{r=0}^{k} \delta_{k,r}^{n} p_{n-k}(x) p_{k-r}(x) p_r(x) \end{pmatrix}. \tag{24}$$

We impose the projective boundary conditions and find a numerical solution to the BVP that is tangent to the unstable and stable subspaces of the linear ODE system

$$\begin{pmatrix} p_n \\ p_n' \end{pmatrix}' = \begin{pmatrix} 0 & 1 \\ 1+\lambda n - 3p_0^2 & 0 \end{pmatrix} \begin{pmatrix} p_n \\ p_n' \end{pmatrix}$$

at $x = \mp\infty$. That is, the boundary conditions are

$$\begin{aligned} P_L \cdot p_n(-L) &= 0 \\ P_R \cdot p_n(L) &= 0, \end{aligned} \tag{25}$$

where $P_L = (-\sqrt{1+\lambda n}, 1)^T$ and $P_R = (\sqrt{1+\lambda} n, 1)^T$.

In solving the Homological equations, we take $L = 20$.

3.4 Gray-Scott's Homological Equations

Recall that the Gray-Scott equations have the unstable eigenvalue $\lambda \approx 8.6267$, and take the profiles u_*, v_* and eigenfunctions as discussed in Section 2.3.2. Since the unstable manifold is one dimensional we make the power series ansatz

$$\vec{P}(\theta, x) = \begin{bmatrix} P(\theta, x) \\ Q(\theta, x) \end{bmatrix} = \sum_{n=0}^{\infty} \begin{bmatrix} u_n(x) \\ v_n(x) \end{bmatrix} \theta^n = \sum_{n=0}^{\infty} \vec{p}_n(x) \theta^n, \tag{26}$$

where $u_0(x) = u_*(x)$, $v_0(x) = v_*(x)$, $u_1(x) = \xi(x)$, and $v_1(x) = \eta(x)$.

In this case the invariance equation reduces to

$$\lambda\theta \frac{\partial}{\partial\theta} \vec{P}(\theta, x) = F(\vec{P}(\theta, x)),$$

where, as before

$$\lambda\theta \frac{\partial}{\partial\theta} \vec{P}(\theta, x) = \sum_{n=0}^{\infty} n\lambda \vec{p}_n(x) \theta^n,$$

and

$$F(\vec{P}(\theta,x)) = \begin{pmatrix} \frac{\partial^2}{\partial x^2}P(\theta,x) - P(\theta,x)Q(\theta,x)^2 + \alpha(1-P(\theta,x)) \\ \frac{\partial^2}{\partial x^2}Q(\theta,x) - \frac{1}{\gamma}Q(\theta,x) + \frac{1}{\gamma}P(\theta,x)Q(\theta,x)^2 \end{pmatrix}.$$

A calculation following the same steps as in Section 3.3 shows that for $n \geq 2$ that the coefficients $\vec{p}_n(x)$ must satisfy,

$$\begin{aligned} u_n''(x) - (\alpha + n\lambda)u_n(x) - v_*(x)^2 u_n(x) - 2u_* v_* v_n(x) &= (u\hat{*}v\hat{*}v)_n, \\ v_n''(x) - n\lambda v_n(x) + \frac{1}{\gamma}\left(v_*(x)^2 u_n(x) + 2u_* v_* v_n(x) - v_n(x)\right) &= -\frac{1}{\gamma}(u\hat{*}v\hat{*}v)_n \end{aligned} \tag{27}$$

which again has the desired from

$$(DF(u_*, v_*) - n\lambda \mathrm{Id})\,\vec{p}_n(x) = R_n(x),$$

and recovers the explicit form of $R_n(x)$.

Introducing the variables $p_n(x) = u_n'(x)$ and $q_n(x) = v_n'(x)$, the homological equations can be rewritten as a first order system, giving rise to the boundary value problem

$$\begin{pmatrix} u_n' \\ p_n' \\ v_n' \\ q_n' \end{pmatrix} = \begin{pmatrix} 0 & 1 & 0 & 0 \\ \alpha + n\lambda + v_*^2 & 0 & u_* v_* & 0 \\ 0 & 0 & 0 & 1 \\ -\frac{v_*^2}{\gamma} & 0 & \frac{1}{\gamma} + n\lambda - \frac{2}{\gamma}u_* v_* & 0 \end{pmatrix} \begin{pmatrix} u_n \\ p_n \\ v_n \\ q_n \end{pmatrix} + \begin{pmatrix} 0 \\ b_n \\ 0 \\ -\frac{1}{\gamma}b_n \end{pmatrix}, \tag{28}$$

where $b_n := (u\hat{*}v\hat{*}v)_n$.

Let

$$A_\pm = \begin{pmatrix} 0 & 1 & 0 & 0 \\ \alpha - n\lambda & 0 & 0 & 0 \\ 0 & 0 & 0 & 1 \\ 0 & 0 & n\lambda & 0 \end{pmatrix},$$

and $W_n(x) = (u_n(x), p_n(x), v_n(x), q_n(x))^T$. Define P_L^1, P_L^2 and P_R^1, P_R^2 to be the unstable eigenvectors of A_- and the stable eigenvectors of A_+ respectively, and let $\mathbb{E}_+ = \mathrm{span}(P_L^1, P_L^2)$ and $\mathbb{E}_- = \mathrm{span}(P_R^1, P_R^2)$. We choose a large $L > 0$ and impose the projected boundary condition $W_n(-L) \in \mathbb{E}_+$ and $W_n(L) \in \mathbb{E}_+$ to numerically solve the homological equation.

3.5 Shrödinger's Homological Equations

Suppose that $u_*(x), v_*(x)$ is an equilibrium (standing wave) solution of the Shrödinger equation with complex conjugate eigenvalues

$$\lambda_{1,2} = \alpha \pm i\beta,$$

and that the corresponding complex conjugate eigenvectors $\xi(x) = (\xi_1(x), \xi_2(x))$, and $\eta(x) = (\eta_1(x), \eta_2(x))$ satisfy

$$\overline{\xi(x)} = \eta(x).$$

Let

$$P(\theta_1, \theta_2, x) = \sum_{m=0}^{\infty} \sum_{n=0}^{\infty} \begin{bmatrix} u_{mn}(x) \\ v_{mn}(x) \end{bmatrix} \theta_1^m \theta_2^n,$$

with

$$u_{00}(x) = u_0(x), \qquad v_{00} = v_0(x),$$

and

$$u_{10}(x) = \xi_1(x), \qquad v_{10} = \xi_2(x), \qquad u_{01}(x) = \eta_1(x) \qquad v_{01} = \eta_2(x),$$

are the components of the eigenfunction. Since the unstable manifold is two dimensional the invariance equation in this case reduces to

$$\lambda_1 \theta_1 \frac{\partial}{\partial \theta_1} P(\theta_1, \theta_2, x) + \lambda_2 \theta_2 \frac{\partial}{\partial \theta_2} P(\theta_1, \theta_2, x) = F(P(\theta_1, \theta_2, x)).$$

Substituting in the power series ansatz leads to

$$\lambda_1 \theta_1 \frac{\partial}{\partial \theta_1} P(\theta_1, \theta_2, x) + \lambda_2 \theta_2 \frac{\partial}{\partial \theta_2} P(\theta_1, \theta_2, x) = \sum_{m=0}^{\infty} \sum_{n=0}^{\infty} (\lambda_1 m + \lambda_2 n) \begin{bmatrix} u_{mn}(x) \\ v_{mn}(x) \end{bmatrix} \theta_1^m \theta_2^n,$$

on the left and

$$F(P(\theta_1, \theta_2, x)) =$$

$$\sum_{m=0}^{\infty} \sum_{n=0}^{\infty} \begin{pmatrix} -v''_{mn}(x) + \mu v_{mn}(x) - (v * v * v)_{mn} - (v * u * u)_{mn} \\ u''_{mn}(x) - u_{mn}(x) + (u * v * v)_{mn} + (u * u * u)_{mn} - 2\nu v_{mn} \end{pmatrix} \theta_1^m \theta_2^n,$$

on the right. Matching like powers leads to

$$(\lambda_1 m + \lambda_2 n) \begin{pmatrix} u_{mn} \\ v_{mn} \end{pmatrix} =$$

$$\begin{pmatrix} -v''_{mn}(x) + \mu v_{mn}(x) - (v * v * v)_{mn} - (v * u * u)_{mn} \\ u''_{mn}(x) - u_{mn}(x) + (u * v * v)_{mn} + (u * u * u)_{mn} - 2\nu v_{mn} \end{pmatrix} =$$

$$\begin{pmatrix} -v''_{mn} + \mu v_{mn} - 3v_*^2 v_{mn} - (v \hat{*} v \hat{*} v)_{mn} - u_*^2 v_{mn} - 2v_* u_* u_{mn} - (v \hat{*} u \hat{*} u)_{mn} \\ u''_{mn} - u_{mn} + 2u_* v_* v_{mn} + v_*^2 u_{mn} + (u \hat{*} v \hat{*} v)_{mn} + 3u_*^2 u_{mn} + (u \hat{*} u \hat{*} u)_{mn} - 2\nu v_{mn} \end{pmatrix}.$$

Observe that (after choosing an appropriate norm) the Fréchet derivative of F at (u_*, v_*) acting on $(u, v)^T$ is

$$DF(u_*, v_*) \begin{bmatrix} u \\ v \end{bmatrix} = \begin{bmatrix} -v'' + \mu v - 3v_*^2 v - 2u_* v_* u - u_*^2 v \\ u'' - u + 2u_* v_* v + v_*^2 u + 3u_*^2 u - 2\nu v \end{bmatrix}$$

so that the homological equations indeed have the form

$$(DF(u_0, v_0) - (m\lambda_1 + n\lambda_2)\mathrm{Id}) \begin{bmatrix} u_{mn} \\ v_{mn} \end{bmatrix} = R_{mn}(x),$$

just as they must. We stress once again that the entire point of going through the formal series calculations above is that we obtain explicitly the expression

$$R_{mn}(x) = \begin{bmatrix} -(u\hat{*}u\hat{*}u)_{mn} - (u\hat{*}v\hat{*}v)_{mn} \\ (v\hat{*}u\hat{*}u)_{mn} - (v\hat{*}v\hat{*}v)_{mn} \end{bmatrix},$$

for the right hand side. That the left hand side comes out correctly provides a convenient check on our work.

Introducing the variables $p_{mn} = u'_{mn}$ and $q_{mn} = v'_{mn}$ and defining the matrices

$$A_{mn}(x) = \begin{pmatrix} 0 & 1 & 0 & 0 \\ 1 - 3u_*(x)^2 - v_*(x)^2 & 0 & (\lambda_1 n + \lambda_2 m) + 2\nu - 2u_*(x)v_*(x) & 0 \\ 0 & 0 & 0 & 1 \\ -(\lambda_1 n + \lambda_m) - 2u_*(x)v_*(x) & 0 & \mu - 3v_*(x)^2 - u_*(x)^2 & 0 \end{pmatrix}$$

we rewrite the homological equations as the linear system

$$\begin{pmatrix} u'_{nm} \\ p'_{nm} \\ v'_{nm} \\ q'_{nm} \end{pmatrix} = A_{mn} \begin{pmatrix} u_{nm} \\ p_{nm} \\ v_{nm} \\ q_{nm} \end{pmatrix} - \begin{pmatrix} 0 \\ N^1_{mn} \\ 0 \\ N^2_{mn} \end{pmatrix}, \tag{29}$$

where

$$N^1_{mn} := (u\hat{*}u\hat{*}u)_{mn} + (u\hat{*}v\hat{*}v)_{mn},$$
$$N^2_{mn} := (v\hat{*}u\hat{*}u)_{mn} + (v\hat{*}v\hat{*}v)_{mn}.$$

The limiting matrix for the linear portion of (29) is given by

$$A_{\pm} = \begin{pmatrix} 0 & 1 & 0 & 0 \\ 1 & 0 & (\lambda_1 n + \lambda_2 m) + 2\nu & 0 \\ 0 & 0 & 0 & 1 \\ -(\lambda_1 n + \lambda_2 m) & 0 & \mu & 0 \end{pmatrix}. \tag{30}$$

Let $W_{mn}(x) = (u_{mn}(x), p_{mn}(x), v_{mn}(x), q_{mn}(x))^T$ and define P^1_L, P^2_L and P^1_R, P^2_R to be the unstable eigenvectors of A_- and the stable eigenvectors of A_+ respectively, and let $\mathbb{E}_+ = \mathrm{span}(P^1_L, P^2_L)$ and $\mathbb{E}_- = \mathrm{span}(P^1_R, P^2_R)$.

4 Numerical implementation and example calculations

Consider again the parabolic PDE

$$u_t = F(u),$$

as discussed in Section 3.2, or any of the generalizations considered in Section 3. In any case F is densely defined on a Hilbert space $\mathcal{H}$. The numerical procedure for computing the unstable manifold parameterization is as follows.

- **Step 1:** Numerically solve the profile equation $F(u) = 0$ to find a standing wave $u_* \in \mathcal{H}$. Let $p_0 = u_*$
- **Step 2:** Suppose that the standing wave is unstable with Morse index M. If $M = 0$ the wave is stable and the unstable manifold is empty. In this case we end the procedure. Otherwise numerically solve the eigenvector problem

  $$DF(p_*)\xi = \lambda\xi,$$

  to find the unstable eigenvalues λ_1, ..., λ_M and associated eigenfunctions ξ_1, ..., $\xi_M \in \mathcal{H}$. Set $p_{e_j} = \xi_j$ where e_j is the vector with a 1 in the j-th component and zeros elsewhere.
- **Step 3:** Check the non-resonance conditions

  $$m_1\lambda_1 + \ldots + m_M\lambda_M \neq \lambda_j,$$

  $(m_1, \ldots, m_M) \in \mathbb{N}^M$ with $m_1 + \ldots m_M \geq 2$, and for each $1 \leq j \leq M$. (This is actually only a finite number of conditions as λ_j are all unstable). If there is a resonance at order $\tilde{N} \geq 2$ choose $N < \tilde{N}$. If there are no resonances then we are free to approximate the parameterization to any desired order $N \geq 2$.
- **Step 4:** For all $(m_1, \ldots, m_M) \in \mathbb{N}^M$ with $m_1 + \ldots + m_M \geq 2$ solve the homological equation

  $$[DF(p_*) - (m_1\lambda_1 + \ldots + m_M\lambda_M)\mathrm{Id}]\, p_{m_1,\ldots,m_M} = R_{m_1,\ldots,m_M},$$

  where $p_{m_1,\ldots,m_M} \in \mathcal{H}$. This is a projected boundary value problem on the line. The equation has a unique solution as there are no resonances up to order N. Return the power series coefficients $p_{m_1,\ldots,m_M}$ for $0 \leq m_1 + \ldots + m_M \leq N$.

We refer to this as *the main algorithm*. The polynomial

$$P^N(x, \theta_1, \ldots, \theta_M) = \sum_{0 \leq m_1 + \ldots + m_M \leq N} p_{m_1,\ldots,m_M}(x)\theta_1^{m_1} \cdot \ldots \cdot \theta_M^{m_M},$$

approximates the unstable manifold to order N.

As a post-processing step we check the a-posteriori error associated with P^N as follows. Choose an allowed error tolerance $\varepsilon \ll 1$ and for some large $K \in \mathbb{N}$ choose some sample points $\{\vec{\theta}_k\}_{k=1}^K \in \mathbb{B}$ throughout the domain of P^N. For some $\tau > 0$ and for each $1 \leq k \leq K$ define $\tilde{\vec{\theta}}_k$ by

$$\tilde{\vec{\theta}}_k = e^{-\Lambda_M \tau} \vec{\theta}_k.$$

Here

$$\Lambda_M = \begin{pmatrix} \lambda_1 & \dots & 0 \\ \vdots & \ddots & \vdots \\ 0 & \dots & \lambda_M \end{pmatrix},$$

is the diagonal matrix of eigenvalues. Compute the quantities

$$\epsilon_k = \|\Phi_{\text{num}}(\tilde{\vec{\theta}}_k, \tau) - P(\vec{\theta}_k)\|_{\mathcal{H}},$$

where Φ_{num} is a numerical integration scheme for the parabolic PDE. We are satisfied with the calculation if

$$\max(\epsilon_1, \dots, \epsilon_K) \leq \varepsilon.$$

If the check fails then we can decrease the size of the box $\mathbb{B} = [-r_1, r_1] \times \dots \times [-r_M, r_M]$ (or decrease the scalings of the eigenfunctions) and rerun the main algorithm. On the other hand it may turn out that the $\epsilon_1, \dots, \epsilon_K$ are all dramatically less than ε. In this case we can increase the size of the domain (or the scalings of the eigenvectors) and run the main algorithm again.

Automatic procedures for choosing optimal scalings for the eigenvectors are discussed in [71]. In the present work we employ the heuristic that the N-th order coefficients should be on the order of machine epsilon or smaller. This is usually enough to guarantee that $\max(\epsilon_1, \dots, \epsilon_K)$ is less than machine epsilon. We refer to the procedure just described as *a-posteriori verrification* for the main algorithm.

4.1 Unstable manifold for Nagumo's Equations

We use (24) in the main algorithm to recursively solve the first $N = 30$ homological equations. The first four generated solutions of the homological equations we denote by p_2, p_3, p_4, and p_5 and they are illustrated in figure 8. These are the Taylor coefficients of the parameterization to order 5. Observe that the 5-th order coefficients already have C^0 norm on the order of 10^{-5}. The maximum absolute value of the final homological equation solution ($N = 30$) is given by 6.290e-21. We choose a domain of $\mathbb{B} = [-2, 2]$ for the parameterization, that is we take $r = 2$.

Figure 9 illustrates what the nonlinear unstable manifold looks like away from the stationary solution.

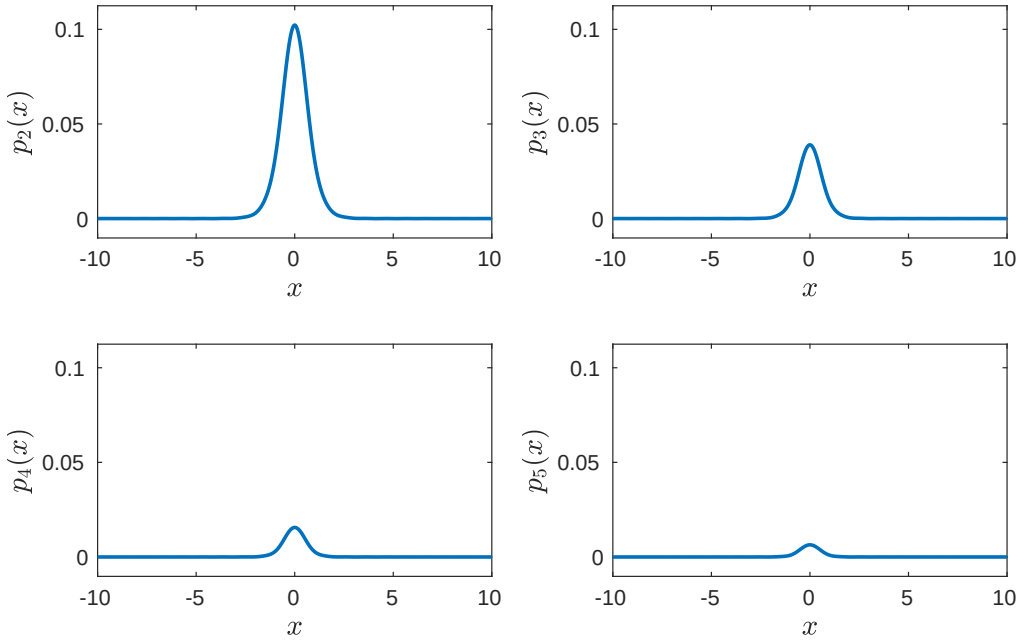

Figure 8: Solutions to the first four generated homological equations, p_2, p_3, p_4, and p_5 for the Nagumo equation.

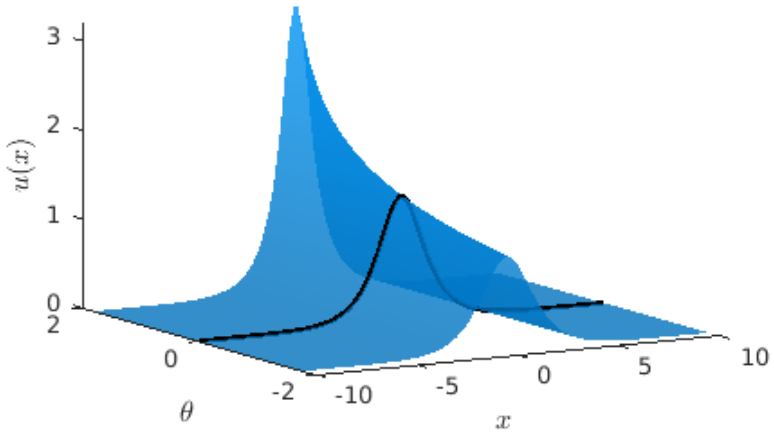

Figure 9: Plot of $u(x)$ on the unstable manifold for Nagumo's equation with values of $\theta \in [-2, 2]$. The black line represents the profile/equilibrium solution.

Δx	Δt	$\|u_n - u_0\|_\infty$
0.02	0.003	0.059127
0.01	0.00075	0.013958
0.005	0.0001875	0.0036251
0.0025	4.6875e-05	0.0010956

Table 1: Convergence study results for Nagumo's equation. Here Δx and Δt represent the grid size in x and t respectively. The last column shows the C^0 norm of the difference between the numerical evolution and the parametrization solution. The integration time $\Delta T = 0.15$ is orders of magnitude larger than the final error.

4.1.1 Finite Difference Verification of Nagumo

To verify the correctness of our approximation we employ the a-posteriori verification scheme for $\hat{\theta}_0 = 1$ and $\hat{\theta}_1 = 1.5683$ respectively. For all systems in this work, we use the package provided in [24] to automatically produce finite difference code for the Crank-Nicolson method, giving the numerical integration scheme Φ_{num}. Recall that the Crank-Nicolson scheme is second order accurate for the heat equation. Thus, we have cause to hope that the Crank-Nicolson scheme will also be second order accurate for the systems we consider. We will consider the parametrized nonlinear manifold to be verified correct if we initialize the finite difference time evolution code with a solution of the parametrization method and then observe convergence of order two of the finite difference scheme solution to the solution predicted by the parametrization after the same amount of time has passed. We remark that the accuracy and speed of the parametrization method compared to the finite difference scheme is one of the benefits of the former. Indeed, the limiting factor in the precision with which we verify the parametrization method is the computation time as the finite difference grid size decreases.

The time elapsed between the two parametrization values θ_0 and θ_1 can be calculated as $\Delta T = (\log(\hat{\theta}_1) - \log(\hat{\theta}_0))/\lambda = 0.15$. We begin the finite difference code at $u_0(x) = P^N(\hat{\theta}_0, x)$ and evolve it ΔT forward in time, denoting its final result as $u_n(x)$. Let $u_1(x) = P^N(\theta_0, x)$. We then can calculate $\|u_n(x) - u_0(x)\|$, the error between the parameterization method and the finite difference method in the C^0 norm.

Using this method, we perform a convergence study for $\Delta x \in \{0.02, 0.01, 5e3, 2.5e\text{-}3\}$ with $\frac{\Delta t}{\Delta x^2} = 0.75$, to see if the finite difference results converge to the solution of the parameterized method as we move toward a tighter mesh. For the time evolution, we use Dirichlet boundary conditions as given by the parametrization method. Here $L = 20$ was our numerical approximation for infinity. We conclude that the method gives accurate results as seen by the rate of convergence shown in Table 1.

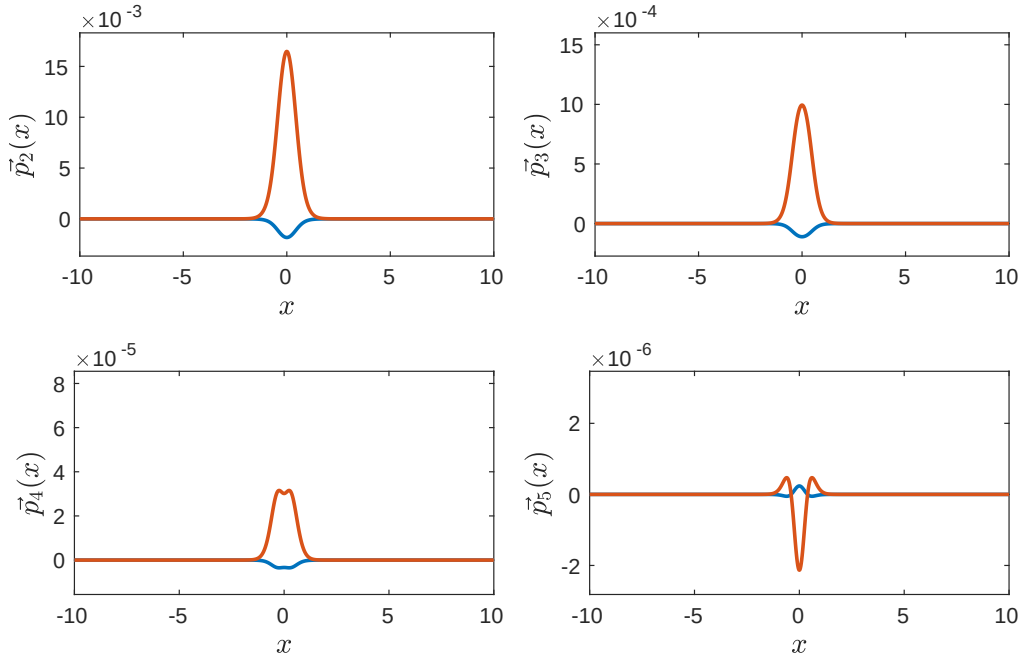

Figure 10: The first four generated homological equations for the Gray Scott equation. Note the scaling decreases in each consecutive figure.

4.2 Unstable manifold for Gray-Scott

We use (28) combined with the main algorithm to recursively solve the first thirty homological equations. Several solutions of the homological equations are shown in Figure 10, a visualization of the manifold is pictured in Figure 11. In solving the homological equations, we take $L = 10$. We compute the parameterization to order $N = 25$ and find that the pointwise-norm (Euclidean norm) over the coefficients of order $N = 25$ is smaller than $1.464e-26$. We choose $r = 10$ so that $\mathbb{B} = [-10, 10]$ is the domain of the parameterization.

4.2.1 Finite Difference Verification of Gray-Scott

Evaluating our parameterization we obtain two solutions, U_0 and U_1, corresponding to values produced by the manifold at $\theta_0 = 1$ and $\theta_1 = 8.6424$ respectively. For our initial state of the finite difference code, we choose U_0. We let ΔT be the total time elapsed by our finite difference method and perform a convergence study by taking $\Delta x \in \{0.1, 0.05, 0.025\}$ with $\frac{\Delta t}{\Delta x^2} = 0.25$ and forming a mesh accordingly. Here $L = 10$, and $N = 30$ is the number of homological equations computed. Table 2 shows the results.

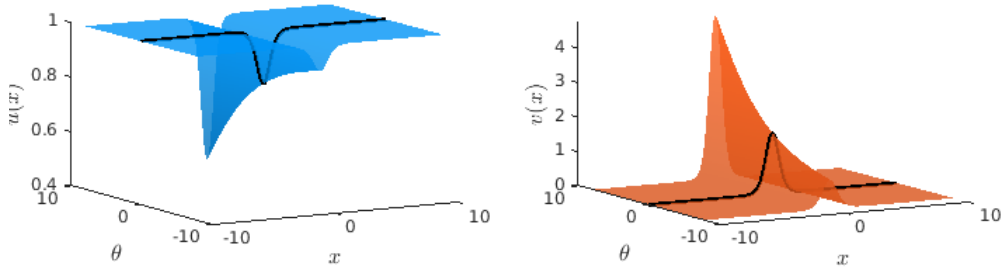

Figure 11: Plot of $u(x)$ and $v(x)$ on the unstable manifold for the Gray-Scot system. Values of $\theta \in [-10, 10]$. The black line represents the profile/equilibrium solution. The u component is in the left frame (blue) while the v component is on the right (red).

Δx	Δt	$\|u_n - u_1\|_\infty$
0.1	2.5e-3	3.62304e-2
0.05	6.25e-4	8.5888e-3
0.025	1.5625e-4	2.1196e-3

Table 2: Convergence study results for Gray Scott. Here Δx is the change in x of the mesh and Δt is the size of each time step. The last column shows the normed difference between the finite difference result and the parameterization result. As the space and time steps are taken smaller, the results appear to converge.

4.3 Unstable manifold for Schrödinger's Equation

We use (29) combined with the main algorithm to solve the first 20 homological equations. That is we compute the parameterization to order $N = 20$. The real and imaginary parts of several of the solutions to the homological equations are shown in Figure 12. To plot the unstable manifold, we require that $\theta_1 = \bar{\theta}_2$ and we vary θ_1 in an outward spiral in the complex plane as shown at the bottom of Figure 13. We also plot the manifold along the image of this spiral reflected across the imaginary axis. In Figure 13, $\theta = |\theta_1|$ along the black spiral, and $\theta = -|\theta_1|$ along the red spiral. Observe that, since the real part of the unstable eigenvalue is positive but small, the linear dynamics is fairly slow. This leads to a substantial oscillation on the manifold. In this case we take $r = 2$ and because we use complex conjugate variables the domain can be thought of as the disk with radius r.

4.3.1 Finite Difference Verification of Shrödinger's Equation

We apply the a-posteriori verification for the main algorithm. We follow the same process as outlined in Section 4.1.1 to perform a convergence study. This time, we choose $\Delta x \in \{0.02, 0.01, 0.005\}$ with $\frac{\Delta t}{\Delta x^2} = 25$. Here $L = 3$, $\Delta T = 1$, $\theta_1 = 1.5 + 1.5i$, and we use 20 homological equations. Table 3 shows the results.

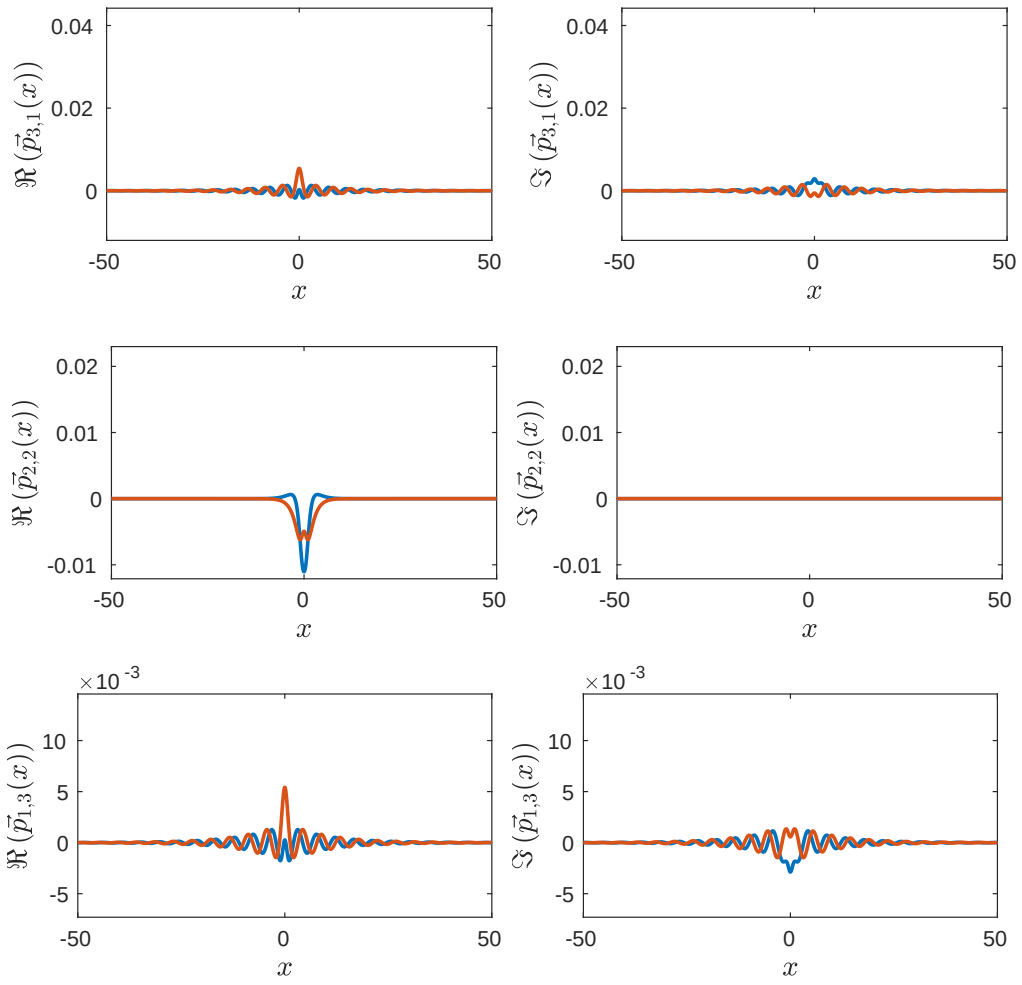

Figure 12: The real and imaginary part of the first four generated homological equations for Shrödinger's equation. Note the scale gets smaller with each subsequent image.

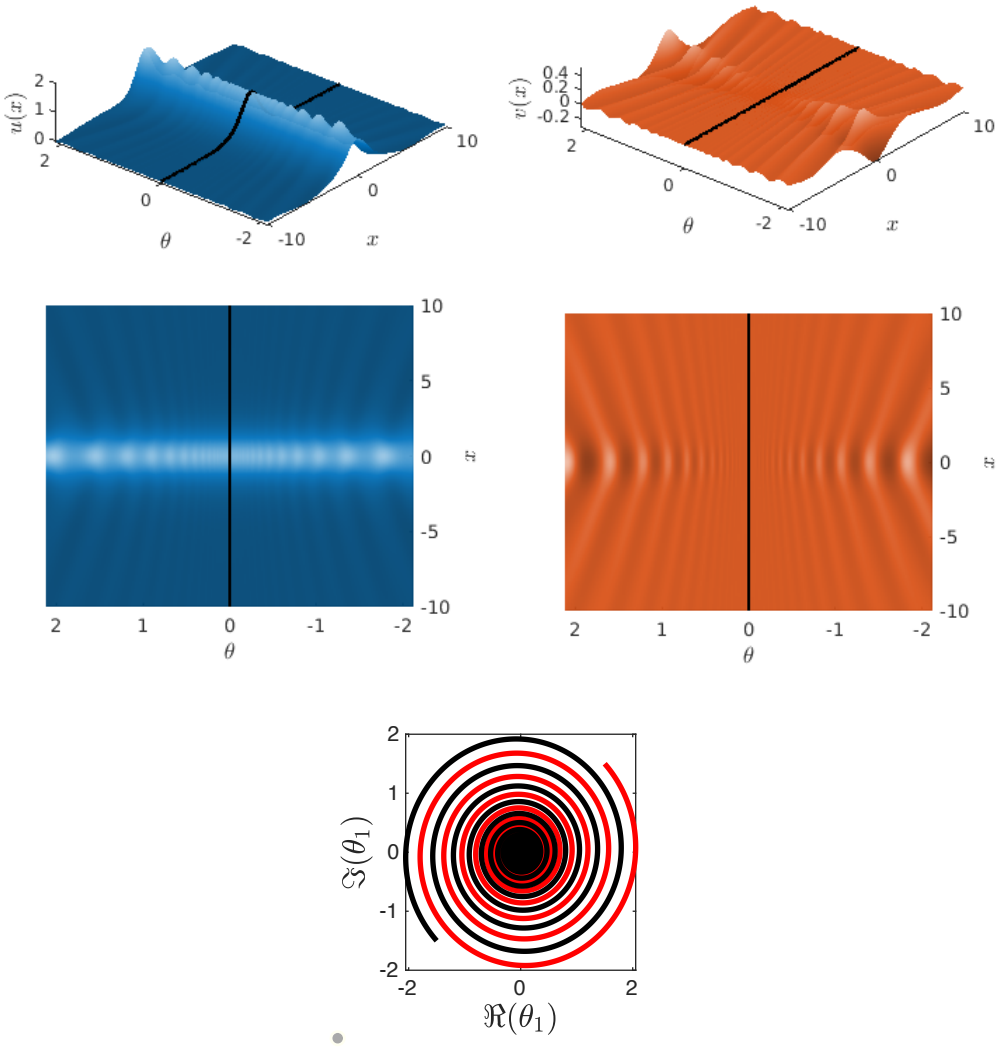

Figure 13: The nonlinear manifold for the Shrödinger equation. Top left and right – $u(x)$ (blue) and $v(x)$ components of a solution on the unstable manifold of the equilibrium. The figure illustrates the oscillation of solutions as they converge (in backward time) to the equilibrium. Center left and right – same as above but a top-down view. Bottom – the corresponding orbit in parameter space. Recall that we are just past a Hopf bifurcation so that the real part of the complex conjugate eigenvalues is fairly small, approximately 0.056. This explains the spiraling in linear dynamics, and accounts for the fairly dramatic oscillation in the solutions on the unstable manifold.

Δx	Δt	$\|u_n - u_1\|_\infty$
0.24	0.016	9.83e-3
0.12	0.004	2.67e-3
0.06	0.001	9.67e-4

Table 3: Convergence study results for Shrödinger's Equation. Here Δx is the change in x of the mesh and Δt is the size of each time step. The last column shows the normed difference between the finite difference result and the parameterization result. As the space and time steps are taken smaller, the results appear to converge. The total integration time in the conjugally check is $\Delta T = 1$ in each case, so that the final error is several magnitudes smaller than the integration time.

5 Conclusions

In this paper we have presented a method for high order numerical approximation of unstable manifolds attached to equilibrium solutions for parabolic PDEs on the line. These equilibria correspond to standing wave solutions of the PDE, and the unstable manifolds describe the time behavior of solutions which diverge from a small neighborhood of the unstable wave. We developed a parameterization method which applies to standing wave solutions and showed that the invariance equation can be solved using formal series methods. We derived the recursion relations, or homological equations, for the formal series solution in a number of example problems and show that the homological equations are non-autonomous systems of linear equations on the line satisfying assymptotic boundary conditions. We implemented numerical methods for solving the homological equations in a number of interesting examples coming from applied mathematics. Using techniques of numerical integration for solving initial value problems for parabolic PDEs on the line we showed that our approximate manifolds provide a good description of the unstable manifolds away from the standing wave.

As already mentioned in Remark 2.2, the methods discussed in the present work apply directly to traveling wave solutions with non-zero wave speed. However we have not considered any such examples in the present work. An interesting future project would be to apply our method to some such examples, computing unstable manifolds attached to traveling kinks and/or pulses. Such a project would require only minor modifications of the techniques described in the present work.

Another interesting generalization would be to study parabolic PDEs formulated on $\mathbb{R}^2$ instead of on the line. For example one could study unstable nonlinear waves for conservation laws. This is an active area of research even in terms of numerical analysis of the wave profiles and their stability, as the traveling wave ansatz does not in general reduce

the problem to an ODE (unless planar waves are considered). It is therefore in general more difficult, if not impossible, to apply dynamical systems techniques. It is nevertheless reasonable to suggest that for any examples where the profile and unstable eigenvalues can be computed numerically, the homological equations for the jets of the parameterization could be developed and solved also numerically. This would make a very interesting topic for a future study.

Finally, we mention that in recent years a number of researchers have developed computer assisted methods of proof for studying existence questions for traveling wave solutions [72, 68, 73, 74] and also computer aided methods for verifying both existence and stability properties of such waves [75, 76, 77, 78, 79]. If one were to develop analogous computer assisted methods of proof for studying the homological equations this would open the way to validated computation of unstable manifolds for traveling waves. Indeed such techniques would be a first step toward computer assisted proofs for connecting orbits in the full PDE (posed on the line), though several other components would be needed as well – namely computer assisted analysis of the stable manifold and computer assisted techniques for rigorous integration of the flow. This is an ambitious program whose completion could take years of sustained research.

6 Thanks

We would like to thank Christian Reinhardt for invaluable conversations and for bringing the first two authors together on this project. We thank Björn Sandstede for making us aware of the explicit eigenvalue-eigenvector pair for the scalar Nagumo equation. The second author was partially supported by NSF grant DMS - 1813501.

References

[1] Blake Barker, Jeffrey Humpherys, Joshua Lytle, and Kevin Zumbrun. STABLAB: A MATLAB-based numerical library for evans function computation. https://github.com/nonlinear-waves/stablab.git.

[2] Xavier Cabré, Ernest Fontich, and Rafael de la Llave. The parameterization method for invariant manifolds. I. Manifolds associated to non-resonant subspaces. *Indiana Univ. Math. J.*, 52(2):283–328, 2003.

[3] Xavier Cabré, Ernest Fontich, and Rafael de la Llave. The parameterization method for invariant manifolds. II. Regularity with respect to parameters. *Indiana Univ. Math. J.*, 52(2):329–360, 2003.

[4] Xavier Cabré, Ernest Fontich, and Rafael de la Llave. The parameterization method for invariant manifolds. III. Overview and applications. *J. Differential Equations*, 218(2):444–515, 2005.

[5] A. Haro and R. de la Llave. A parameterization method for the computation of invariant tori and their whiskers in quasi-periodic maps: explorations and mechanisms for the breakdown of hyperbolicity. *SIAM J. Appl. Dyn. Syst.*, 6(1):142–207, 2007.

[6] À. Haro and R. de la Llave. A parameterization method for the computation of invariant tori and their whiskers in quasi-periodic maps: numerical algorithms. *Discrete Contin. Dyn. Syst. Ser. B*, 6(6):1261–1300, 2006.

[7] A. Haro and R. de la Llave. A parameterization method for the computation of invariant tori and their whiskers in quasi-periodic maps: rigorous results. *J. Differential Equations*, 228(2):530–579, 2006.

[8] Marta Canadell and Àlex Haro. Computation of quasi-periodic normally hyperbolic invariant tori: algorithms, numerical explorations and mechanisms of breakdown. *J. Nonlinear Sci.*, 27(6):1829–1868, 2017.

[9] Marta Canadell and Àlex Haro. Parameterization method for computing quasi-periodic reducible normally hyperbolic invariant tori. In *Advances in differential equations and applications*, volume 4 of *SEMA SIMAI Springer Ser.*, pages 85–94. Springer, Cham, 2014.

[10] Renato C. Calleja, Alessandra Celletti, and Rafael de la Llave. A KAM theory for conformally symplectic systems: efficient algorithms and their validation. *J. Differential Equations*, 255(5):978–1049, 2013.

[11] Gemma Huguet, Rafael de la Llave, and Yannick Sire. Computation of whiskered invariant tori and their associated manifolds: new fast algorithms. *Discrete Contin. Dyn. Syst.*, 32(4):1309–1353, 2012.

[12] Ernest Fontich, Rafael de la Llave, and Yannick Sire. A method for the study of whiskered quasi-periodic and almost-periodic solutions in finite and infinite dimensional Hamiltonian systems. *Electron. Res. Announc. Math. Sci.*, 16:9–22, 2009.

[13] Xiaolong He and Rafael de la Llave. Construction of quasi-periodic solutions of state-dependent delay differential equations by the parameterization method I: Finitely differentiable, hyperbolic case. *J. Dynam. Differential Equations*, 29(4):1503–1517, 2017.

[14] Xiaolong He and Rafael de la Llave. Construction of quasi-periodic solutions of state-dependent delay differential equations by the parameterization method II: Analytic case. *J. Differential Equations*, 261(3):2068–2108, 2016.

[15] Antoni Guillamon and Gemma Huguet. A computational and geometric approach to phase resetting curves and surfaces. *SIAM J. Appl. Dyn. Syst.*, 8(3):1005–1042, 2009.

[16] Gemma Huguet and Rafael de la Llave. Computation of limit cycles and their isochrons: fast algorithms and their convergence. *SIAM J. Appl. Dyn. Syst.*, 12(4):1763–1802, 2013.

[17] John Rinzel and Gemma Huguet. Nonlinear dynamics of neuronal excitability, oscillations, and coincidence detection. *Comm. Pure Appl. Math.*, 66(9):1464–1494, 2013.

[18] Roberto Castelli, Jean-Philippe Lessard, and J. D. Mireles James. Parameterization of invariant manifolds for periodic orbits I: Efficient numerics via the Floquet normal form. *SIAM J. Appl. Dyn. Syst.*, 14(1):132–167, 2015.

[19] J. D. Mireles James and Maxime Murray. Chebyshev-Taylor parameterization of stable/unstable manifolds for periodic orbits: implementation and applications. *Internat. J. Bifur. Chaos Appl. Sci. Engrg.*, 27(14):1730050, 32, 2017.

[20] Àlex Haro, Marta Canadell, Jordi-Lluís Figueras, Alejandro Luque, and Josep-Maria Mondelo. *The parameterization method for invariant manifolds*, volume 195 of *Applied Mathematical Sciences*. Springer, [Cham], 2016. From rigorous results to effective computations.

[21] C. M. Groothedde and J. D. Mireles James. Parameterization method for unstable manifolds of delay differential equations. *J. Comput. Dyn.*, 4(1-2):21–70, 2017.

[22] Christian Reinhardt and J. D. Mireles James. Fourier-Taylor parameterization of unstable manifolds for parabolic partial differential equations: formalism, implementation and rigorous validation. *Indag. Math. (N.S.)*, 30(1):39–80, 2019.

[23] Jorge Gonzalez, Necibe Tuncer, and J. D. Mireles James. Finite element approximation of invariant manifolds by the parameterization method. *(Submitted)*, 2019.

[24] R. Todd and Jalen Morgan. Automated finite-difference time evolution code for conservation laws. *Minnesota Journal of Undergraduate Mathematics*, 4(1), 2019.

[25] G. Haller. Homoclinic jumping in the perturbed nonlinear Schrödinger equation. *Comm. Pure Appl. Math.*, 52(1):1–47, 1999.

[26] G. Haller, G. Menon, and V. M. Rothos. Šilnikov manifolds in coupled nonlinear Schrödinger equations. *Phys. Lett. A*, 263(3):175–185, 1999.

[27] Feng Shan Bai, Alastair Spence, and Andrew M. Stuart. The numerical computation of heteroclinic connections in systems of gradient partial differential equations. *SIAM J. Appl. Math.*, 53(3):743–769, 1993.

[28] Feng Shan Bai, Alastair Spence, and Andrew M. Stuart. Numerical computations of coarsening in the one-dimensional Cahn-Hilliard model of phase separation. *Phys. D*, 78(3-4):155–165, 1994.

[29] F. Christiansen, P. Cvitanović, and V. Putkaradze. Spatiotemporal chaos in terms of unstable recurrent patterns. *Nonlinearity*, 10(1):55–70, 1997.

[30] Yueheng Lan and Predrag Cvitanović. Unstable recurrent patterns in Kuramoto-Sivashinsky dynamics. *Phys. Rev. E (3)*, 78(2):026208, 12, 2008.

[31] D. Viswanath and P. Cvitanović. Stable manifolds and the transition to turbulence in pipe flow. *J. Fluid Mech.*, 627:215–233, 2009.

[32] Predrag Cvitanović, Ruslan L. Davidchack, and Evangelos Siminos. On the state space geometry of the Kuramoto-Sivashinsky flow in a periodic domain. *SIAM J. Appl. Dyn. Syst.*, 9(1):1–33, 2010.

[33] J. Halcrow, J. F. Gibson, P. Cvitanović, and D. Viswanath. Heteroclinic connections in plane Couette flow. *J. Fluid Mech.*, 621:365–376, 2009.

[34] C. Foias, M. S. Jolly, I. G. Kevrekidis, G. R. Sell, and E. S. Titi. On the computation of inertial manifolds. *Phys. Lett. A*, 131(7-8):433–436, 1988.

[35] M. S. Jolly, I. G. Kevrekidis, and E. S. Titi. Approximate inertial manifolds for the Kuramoto-Sivashinsky equation: analysis and computations. *Phys. D*, 44(1-2):38–60, 1990.

[36] M. S. Jolly. Bifurcation computations on an approximate inertial manifold for the 2D Navier-Stokes equations. *Phys. D*, 63(1-2):8–20, 1993.

[37] M. S. Jolly, R. Rosa, and R. Temam. Accurate computations on inertial manifolds. *SIAM J. Sci. Comput.*, 22(6):2216–2238, 2000.

[38] Y.-M. Chung and M. S. Jolly. A unified approach to compute foliations, inertial manifolds, and tracking solutions. *Math. Comp.*, 84(294):1729–1751, 2015.

[39] A. J. Roberts. The application of centre-manifold theory to the evolution of systems which vary slowly in space. *J. Austral. Math. Soc. Ser. B*, 29(4):480–500, 1988.

[40] A. J. Roberts. The utility of an invariant manifold description of the evolution of a dynamical system. *SIAM J. Math. Anal.*, 20(6):1447–1458, 1989.

[41] G. N. Mercer and A. J. Roberts. A centre manifold description of contaminant dispersion in channels with varying flow properties. *SIAM J. Appl. Math.*, 50(6):1547–1565, 1990.

[42] Xiaopeng Chen, Anthony J. Roberts, and Jinqiao Duan. Centre manifolds for infinite dimensional random dynamical systems. *Dyn. Syst.*, 34(2):334–355, 2019.

[43] George Haller and Sten Ponsioen. Nonlinear normal modes and spectral submanifolds: existence, uniqueness and use in model reduction. *Nonlinear Dynam.*, 86(3):1493–1534, 2016.

[44] Robert Szalai, David Ehrhardt, and George Haller. Nonlinear model identification and spectral submanifolds for multi-degree-of-freedom mechanical vibrations. *Proc. A.*, 473(2202):20160759, 19, 2017.

[45] George Haller and Sten Ponsioen. Exact model reduction by a slow-fast decomposition of nonlinear mechanical systems. *Nonlinear Dynam.*, 90(1):617–647, 2017.

[46] Florian Kogelbauer and George Haller. Rigorous model reduction for a damped-forced nonlinear beam model: an infinite-dimensional analysis. *J. Nonlinear Sci.*, 28(3):1109–1150, 2018.

[47] Thomas Breunung and George Haller. Explicit backbone curves from spectral submanifolds of forced-damped nonlinear mechanical systems. *Proc. A.*, 474(2213):20180083, 25, 2018.

[48] Bernd Krauskopf and Kirk Green. Computing unstable manifolds of periodic orbits in delay differential equations. *J. Comput. Phys.*, 186(1):230–249, 2003.

[49] B. Krauskopf, K. Green, and K. Engelborghs. From local to global one-dimensional unstable manifolds in delay differential equations. In *EQUADIFF 2003*, pages 175–180. World Sci. Publ., Hackensack, NJ, 2005.

[50] Pieter Collins and Bernd Krauskopf. Chaotic lasers: manifolds, bifurcations and symbolic dynamics. In *EQUADIFF 2003*, pages 871–876. World Sci. Publ., Hackensack, NJ, 2005.

[51] Kirk Green, Bernd Krauskopf, and Koen Engelborghs. One-dimensional unstable eigenfunction and manifold computations in delay differential equations. *J. Comput. Phys.*, 197(1):86–98, 2004.

[52] R. C. Calleja, A. R. Humphries, and B. Krauskopf. Resonance phenomena in a scalar delay differential equation with two state-dependent delays. *SIAM J. Appl. Dyn. Syst.*, 16(3):1474–1513, 2017.

[53] Michael Dellnitz, Mirko Hessel-Von Molo, and Adrian Ziessler. On the computation of attractors for delay differential equations. *J. Comput. Dyn.*, 3(1):93–112, 2016.

[54] Jan Bouwe van den Berg, Jason D. Mireles James, and Christian Reinhardt. Computing (un)stable manifolds with validated error bounds: Non-resonant and resonant spectra. *Journal of Nonlinear Science*, 26(4):1055–1095, Apr 2016.

[55] Jean-Philippe Lessard, Jason D. Mireles James, and Christian Reinhardt. Computer assisted proof of transverse saddle-to-saddle connecting orbits for first order vector fields. *J. Dynam. Differential Equations*, 26(2):267–313, 2014.

[56] Blake Barker, Heinrich Freistühler, and Kevin Zumbrun. Convex entropy, hopf bifurcation, and viscous and inviscid shock stability. *Arch. Rational Mech. Anal.*, 2015.

[57] Blake Barker, Marta Lewicka, and Kevin Zumbrun. Existence and stability of viscoelastic shock profiles. *Arch. Ration. Mech. Anal.*, 200(2):491–532, 2011.

[58] R. A. Gardner and C. K. R. T. Jones. Traveling waves of a perturbed diffusion equation arising in a phase field model. *Indiana Univ. Math. J.*, 39(4):1197–1222, 1990.

[59] Anna Ghazaryan, Yuri Latushkin, and Stephen Schecter. Stability of traveling waves for degenerate systems of reaction diffusion equations. *Indiana University Mathematics Journal*, 60(2):443–471, 2011.

[60] Björn Sandstede. Evans functions and nonlinear stability of traveling waves in neuronal network models. *International Journal of Bifurcation and Chaos*, 17(08):2693–2704, Aug 2007.

[61] Eusebius J. Doedel and Mark J. Friedman. Numerical computation of heteroclinic orbits. *J. Comput. Appl. Math.*, 26(1-2):155–170, 1989. Continuation techniques and bifurcation problems.

[62] Eusebius Doedel. AUTO: a program for the automatic bifurcation analysis of autonomous systems. *Congr. Numer.*, 30:265–284, 1981.

[63] B. Barker, J. Humpherys, G. Lyng, and J. Lytle. Evans function computation for the stability of travelling waves. *Philos. Trans. Roy. Soc. A*, 376(2117):20170184, 25, 2018.

[64] Blake Barker, Rose Nguyen, Björn Sandstede, Nathaniel Ventura, and Colin Wahl. Computing Evans functions numerically via boundary-value problems. *Phys. D*, 367:1–10, 2018.

[65] Jeffrey Humpherys and Joshua Lytle. Root following in Evans function computation. *SIAM J. Numer. Anal.*, 53(5):2329–2346, Jan 2015.

[66] P. Gray and S. K. Scott. Autocatalytic reactions in the isothermal, continuous stirred tank reactor: Oscillations and instabilities in the system A + 2B $\rightarrow$ 3B, B $\rightarrow$ C. *Chem. Engrg. Sci*, 39:1087–1097, 1984.

[67] J. K. Hale, L. A. Peletier, and W. C. Troy. Exact homoclinic and heteroclinic solutions of the Gray-Scott model for autocatalysis. *SIAM J. Appl. Math*, 61(1):102–130, 2000.

[68] Jan Bouwe van den Berg, Jason D. Mireles-James, Jean-Philippe Lessard, and Konstantin Mischaikow. Rigorous numerics for symmetric connecting orbits: even homoclinics of the Gray-Scott equation. *SIAM J. Math. Anal*, 43(4):1557–1594, 2011.

[69] Arjen Doelman, Robert A. Gardner, and Tasso J. Kaper. Stability analysis of singular patterns in the 1d gray-scott model: a matched asymptotics approach. *Physica D: Nonlinear Phenomena*, 122(1-4):1–36, Nov 1998.

[70] Paul C. Chang. Modulation stability of oscillatory pulse soluitons of the parameterically-forced nonlinear Schrödinger equation. Master's thesis, Simon Fraser University, July 2001.

[71] Maxime Breden, Jean-Philippe Lessard, and Jason D. Mireles James. Computation of maximal local (un)stable manifold patches by the parameterization method. *Indag. Math. (N.S.)*, 27(1):340–367, 2016.

[72] Oswald Fogelklou, Warwick Tucker, and Gunilla Kreiss. A computer-assisted proof of the existence of traveling wave solutions to the scalar Euler equations with artificial viscosity. *NoDEA Nonlinear Differential Equations Appl.*, 19(1):97–131, 2012.

[73] Jan Bouwe van den Berg, Andréa Deschênes, Jean-Philippe Lessard, and Jason D. Mireles James. Stationary coexistence of hexagons and rolls via rigorous computations. *SIAM J. Appl. Dyn. Syst.*, 14(2):942–979, 2015.

[74] István Balázs, Jan Bouwe van den Berg, Julien Courtois, János Dudás, Jean-Philippe Lessard, Anett Vörös-Kiss, J. F. Williams, and Xi Yuan Yin. Computer-assisted proofs for radially symmetric solutions of PDEs. *J. Comput. Dyn.*, 5(1-2):61–80, 2018.

[75] Blake Barker. *Numerical proof of stability of roll waves in the small-amplitude limit for inclined thin film flow*. ProQuest LLC, Ann Arbor, MI, 2014. Thesis (Ph.D.)–Indiana University.

[76] Blake Barker. Numerical proof of stability of roll waves in the small-amplitude limit for inclined thin film flow. *J. Differential Equations*, 257(8):2950–2983, 2014.

[77] Gianni Arioli and Hans Koch. Existence and stability of traveling pulse solutions of the FitzHugh-Nagumo equation. *Nonlinear Anal.*, 113:51–70, 2015.

[78] Blake Barker and Kevin Zumbrun. Numerical proof of stability of viscous shock profiles. *Math. Models Methods Appl. Sci.*, 26(13):2451–2469, 2016.

[79] Matthew Creek, Roland Donninger, Wilhelm Schlag, and Stanley Snelson. Linear stability of the skyrmion. *Int. Math. Res. Not. IMRN*, 2017(8):2497–2537, 2017.